JOURNAL OF GEOPHYSICAL RESEARCH, VOL. 86, NO. B4, PAGES 2971-3001, APRIL 10, 1981

Ascent and Eruption of Basaltic Magma on the Earth and Moon

LIONEL WILSON[1]

Lunar and Planetary Unit, Department of Environmental Sciences, University of Lancaster Lancaster, LA1 4YQ, United Kingdom

JAMES W. HEAD III

Department of Geological Sciences, Brown University, Providence, Rhode Island 02912

Geological and physical observations and constraints are applied to the development of a model of the ascent and emplacement of basaltic magma on the earth and moon. Mathematical models of the nature and motion of gas/liquid mixtures are developed and show that gas exsolution from terrestrial and lunar magmas commonly only occurs at shallow depths (less than 2 km); thus the ascent of bubble-free magma at depth can be treated separately from the complex motions caused by gas exsolution near the surface. Magma ascent is related to dike or conduit width; a lower limit to width is determined by the presence of a finite magma yield strength or by excessive magma cooling effects related to magma viscosity. For terrestrial basalts with negligible yield strengths and viscosities greater than 10^2 Pa s, widths in the range 0.2–0.6 m are needed to allow eruptions from between depths of 0.5–20 km. Fissure widths of about 4 m would be needed to account for the output rates estimated for the Columbia River flood basalt eruptions. As the magma nears the surface, bubble coalescence will tend to occur, leading to intermittent explosive strombolian-style activity. For commonly occurring lunar and terrestrial basalts the magma rise speed must be greater than 0.5–1 m/s if strombolian activity is to be avoided and relatively steady fire fountaining is to take place. Terrestrial fire fountain heights are dictated by the vertical velocity of the magma/gas dispersion emerging through the vent, increasing with increasing magma gas content and mass eruption rate, and decreasing with increasing magma viscosity. Terrestrial fire fountain heights up to 500 m imply the release of up to 0.4 wt % water from the magma, corresponding to initial water contents up to 0.6 wt %. The presence of extremely long lava flows and sinuous rilles on the moon has often been cited as evidence for very high extrusion rates and thus a basic difference between terrestrial and lunar magmas and crustal environments. However, the differences between terrestrial and lunar magma rheologies and crustal environments do not lead to gross differences between the effusion rates expected on the two planetary bodies, for similar-sized conduits or fissures. Thus the presence of these features implies only that tectonic and other forces associated with the onset of some lunar eruptions were such as to allow wide fissures or conduits to form. The surface widths of elongate fissure vents need be no wider than 10 m to allow mass eruption rates up to 10 times larger than those proposed for terrestrial flood basalt eruptions; 25-m widths would allow rates 100 times larger. It therefore appears unlikely that source vents on the moon with widths greater than a few tens of meters represent the true size of the unmodified vent. The main volatile released from lunar magmas was probably carbon monoxide, released in amounts proportionally less than terrestrial magmas by more than an order of magnitude. However, decompression to the near-zero ambient lunar atmospheric pressure causes much greater energy release per unit mass and this, coupled with vertical and horizontal expansion of the gas, suggests a much more efficient use of the available gas on the moon than on the earth. Some amount of magma disruption must always have taken place in lunar eruptions unless the gas content was truly zero or the magma possessed an appreciable yield strength. Pyroclastic deposits, such as the extensive lunar dark mantling material, could be produced from a single source vent and extend to diameters of up to 200 km. Such deposits could result either from steady eruptions at high effusion rates (with less than 1% of the magma disrupted into submillimeter droplets) or low effusion rate eruptions in which strombolian activity occurred. The wide dispersal of pyroclastic debris is a result of small particles being locked into the expanding gas cloud. Finally, we consider the details of basaltic eruption processes on the moon and predict the nature and geometry of several types of volcanic landforms (flows, pyroclastic blankets and cones, cinder and spatter ridges, etc.) that should result from specific eruption conditions.

I. INTRODUCTION

In this paper we attempt to draw together various ideas concerning the eruption of, principally, basaltic liquids on planets and to obtain detailed relationships giving the dependence of the magma rise speed and mass eruption rate in open conduits on both the magma properties (viscosity, density, yield strength, volatile content, and composition) and the parameters of the conduit system (fissure width and length, source region depth, planetary gravity, and lithostatic pressure gradient). We consider only direct eruption to the surface of magma stored in a reservoir at depth; we are not concerned here with the emplacement of such reservoirs by ascent of large magma bodies through the lithosphere (which has been studied by *Weertman* [1971*a*], *Fedotov* [1977*b*], *Marsh* [1978], and *Marsh and Kantha* [1978]) or with the propagation of cracks to form dikes or sills before the onset of an eruption (treated by *Weertman* [1971*b*], *Johnson and Pollard* [1973], and *Pollard and Muller* [1976].).

A number of important aspects of the eruption process have been treated before. *Shaw and Swanson* [1970] derived the rise velocity of a gas-free Newtonian liquid in a fissure as part of an analysis of terrestrial flood-basalt eruptions, and *Housley* [1978] examined several aspects of the expected differences between basaltic eruptions on the earth and moon. *Fedotov* [1978] summarized and extended work by several authors on

[1] Currently at Department of Geological Sciences, Brown University, Providence, Rhode Island 02912.

Paper number 80B1254.
0148-0227/81/080B-1254$01.00

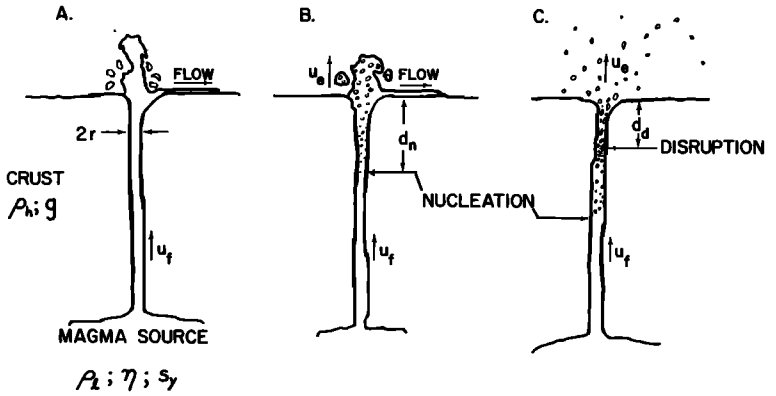

Fig. 1. Basic geometry of fissure or conduit system used in simulated eruptions. Three cases are shown: (*a*) gas-free eruption; (*b*) eruption in which gas is exsolved but gas volume fraction never reaches a large enough value to disrupt magma; (*c*) eruption in which gas volume becomes so large that magma is disrupted into a spray of gas and pyroclasts. The variables are defined in the text.

the cooling by heat loss to the surroundings of a rising, gas-free, terrestrial Newtonian magma; he also reviewed the effects of heat generation by viscous dissipation in such a liquid. *Hardee and Larson* [1977] improved the treatment of the latter problem. *Johnson and Pollard* [1973] studied the motion of gas-free Newtonian, Bingham, and pseudoplastic liquids in dikes and sills. *Delaney and Pollard* [1980] have treated the time-dependent aspects of the cooling of a liquid (not necessarily Newtonian) flowing in a dike. *Solomon* [1975] proposed a model based on hydrostatic arguments for the eruption of gas-free lunar mare basalts, and *Davies and Stephenson* [1977] calculated some values for the rise rates of such magmas under low Reynolds number, laminar flow conditions.

Several complications appear when the possibility of gas exsolution in the magma is permitted. *McGetchin and Ullrich* [1973] gave solutions (for several planets) for the case of the rise of a mixture of released gas and disrupted magma driven by an exactly lithostatic pressure gradient in a diatreme. *Pai et al.* [1978] treated the same problem for a particular set of lunar conditions, introducing explicitly the effective acoustic velocity in the erupting mixture. *Steinberg and Steinberg* [1975] and *Housley* [1978] explored the significance of the acoustic velocity as a limit on the eruption speed. *Wilson et al.* [1980] studied the general case of the rise of a rhyolitic magma under terrestrial conditions, treating each of the following stages in the motion: rise of gas-free Newtonian liquid; onset of water or carbon dioxide exsolution, bubble growth to the point of magma disruption, rise of gas/clast dispersion, and supersonic transition in a vent of suitable shape. We extend this analysis to include a variety of likely volatile species exsolved from a magma with any viscosity and use studies of bubble rise by *Sparks* [1978] to define the boundary between intermittently explosive strombolian activity and steady fire-fountaining. A major aim of this analysis is the prediction of the ranges of conditions under which the various types of lunar basaltic volcanic features were formed.

II. Basic Concepts of Magma Rise

A. Geological Constraints

A melt which is less dense than its surroundings will tend to rise in a gravitational field. In the deep crust or upper mantle it may rise diapirically [*Ramberg,* 1967; *Elder,* 1976; *Fedotov,* 1977*b*; *March,* 1978; *Marsh and Kantha,* 1978]: the surrounding material deforms out of the way. Nearer the surface it may find a pathway via a fissure opened by tectonic forces (which may or may not be associated with the magma generating events [*Weertman,* 1971*b*]), or it may produce its own fissure by hydraulic fracturing [*Johnson and Pollard,* 1973] if there is an adequate local excess pressure in the magma. Such pressures may be up to 200 bars [*Popov,* 1973]; *Wadge* [1977] found values up to 150 bars to be applicable to flank eruptions on Mount Etna, while *Aki et al.* [1977] inferred values of about 20 bars for magma motion under Kilauea. The source of such excess pressure may be the density difference between the magma and the surrounding rocks or may be some nonhydrostatic process: examples include convective creep of deep materials [*Elder,* 1976], volume changes on melting [*Fedotov,* 1977*a*], and gas exsolution after convective stirring [*Sparks et al.,* 1978] or as a result of partial crystallization of the magma.

If a fissure is produced tectonically, the width will depend on the amount of stress to be relieved and the horizontal extent of the strained region; similarly, the length depends on the detailed prefracture stress distribution, and it is difficult to predict the expected width to length ratio. *Fedotov* [1978] has summarized work on the expected shape of hydraulic fractures and finds width to length ratios in the range 10^{-2} to 10^{-3} in near-surface layers and in the range 10^{-3} to 10^{-4} in the deep crust.

As an eruption proceeds, fissure widening may occur as a result of wall erosion; however, if a fissure initially opens as a result of a large excess (nonhydrostatic) pressure in the source region, then fissure closure may occur as the excess pressure is relieved. Since erosion of fissure walls is likely to be greatest in those regions where the magma rise velocity is greatest, the tendency will be toward localization of the flow of the sheet of rising magma in a long, narrow fissure into a small number of discrete, vertical zones. Since, as we shall find shortly (equations (13) and (14) below), the rise velocity is proportional to (fissure width)^2 for low velocity, laminar flow in a narrow fissure and is proportional to (fissure width)$^{1/2}$ for high velocity, turbulent flow in a wide fissure, the flow localization process may be most important early on in an eruption, as was observed, for example, in the case of the 1973 eruption of Heimaey, Iceland [*Thorarinsson et al.,* 1973].

We are mainly concerned, in this paper, with relationships between magma properties and fissure geometry on the one hand and magma rise speed and mass flow rate on the other.

The mass flow rate is defined as the mass of magma per unit time crossing any horizontal plane cutting the fissure; continuity requires that the mass flow rate in the fissure system be equal to the mass erupted per unit time from the surface vent. The latter is often expressed as an effusion rate in units of magma volume per unit time and may be converted to a mass eruption rate by multiplying by the magma density. Since rise velocity is controlled, via wall friction, by the width of a fissure while mass flow rate depends on both the width and the horizontal length (and can be made arbitrarily large by assuming a very long fissure of any given width), it follows that the largest rise velocity for a given mass flow rate will be that which occurs through a short fissure of any given width; the extreme example of such a geometry is flow in a circular conduit (for which the length is equal to the width), and we shall treat this case initially, commenting on the properties of long fissures as necessary.

Magma will not reach the surface at all through a fissure which is narrower than a certain width or a conduit which is smaller than a certain diameter, the limit being set by either cooling effects or the presence of a yield strength in the magma. (Magma is said to have a yield strength if a finite stress must be applied to it in order to cause flow to occur; Newtonian liquids have zero yield strength.) There is no simple theoretical upper limit to magma rise speed; the limit will be set via frictional effects by the width or diameter of the largest fissure or conduit produced during the eruption. This will be related to the size of tectonic forces if erosion is not important or to the size of the available magma source body and hence eruption duration if erosion does occur.

The pressure at any depth in an erupting magma is not likely to be greatly different from the local lithostatic pressure once steady flow to the surface has been established. If an eruption is initiated by an excess pressure in a magma body, the overlying rocks will fail when their tensile strength or shear strength is exceeded. Similarly, if the pressure in an already erupting magma differs from the stress in the surrounding rocks by a sufficient amount, wall failure will occur. The strength is likely to be low in the deep crust where rocks can deform plastically (and where high stress differentials are unlikely to accumulate), low in unconsolidated near-surface layers and highest at intermediate levels in the crust—though the numerical value of the pressure difference is unlikely to be greater than 200 bars at any depth as noted above. In the immediate vicinity of a volcanic vent, accumulating eruption products may be in the form of loose pyroclastic fragments or liquid lava. Preexisting surface materials may be fragmented debris or old volcanic rocks broken by cooling joints or, on any atmosphereless body, an impact-generated regolith. All of these materials have essentially zero strength compared with lithostatic pressures, and so it is very likely that the pressure in an erupting volcanic fluid will become lithostatic over at least the last few tens of meters soon after an eruption starts. Even where absolute pressures differ from lithostatic values by a few tens of bars deeper in a conduit system, the pressure gradient, which is the driving mechanism for the eruption, will be close to the lithostatic gradient, and the two will be assumed equal in most of our calculations.

Figure 1 shows the geometry of the conduit and fissure systems treated and defines several of the variables needed. At depths great enough that no gas is exsolved (or at all depths for a gas-free magma) the magmatic liquid is assumed to have density ρ_l, viscosity η, and yield strength s_y. It rises through a circular conduit of diameter $2r$ or through an elongate rectangular fissure with width $2r$ and length L. The surrounding crust has constant density ρ_h, and the acceleration due to gravity is g, so that at depth h below the surface the lithostatic pressure is $P = \rho_h g h$. If any gas is exsolved from the magma, it first nucleates at depth d_n; if enough gas exsolves before a given part of the magma reaches the surface, bubbles will grow to a close-packed condition and magma disruption will occur [*Sparks*, 1978] at a depth d_d. The magma rise speed will be a constant u_f in the gas-free region if r does not vary systematically with depth (see below); the vertical velocity of the eruption products in the vent will be denoted u_e when gas is present.

B. *Physical Constraints*

The energy equation for a moving Newtonian fluid in which the spatial flow field does not change appreciably with time may be written [*McGetchin and Ullrich*, 1973]

$$-\int \frac{dP}{\rho} = \int u\,du - \int g\,dh - \int \frac{fu^2}{4r}\,dh \tag{1}$$

where u and ρ are the local mean values of the magma rise velocity and density and f is a friction factor. The motion is one dimensional in the sense that the mean values of the variables are functions only of the depth h. At low Reynolds numbers in the laminar flow regime, f is inversely proportional to the Reynolds number Re given by

$$Re = 2ru\rho/\eta \tag{2}$$

while at high Reynolds numbers, in turbulent flow, f tends to a constant which depends only on wall roughness. An adequate approximate expression for f is [*Wilson et al.*, 1980]

$$f = \frac{A}{Re} + K \tag{3}$$

where K is about 0.01 under most circumstances and $A = 64$ for a circular tube, $A = 24$ for a long fissure [e.g., *Schlichting*, 1968].

The mass eruption rate in the case of a circular tube is M given by

$$M = \rho u \pi r^2 \tag{4}$$

and the continuity condition $dM/dh = 0$ implies

$$\frac{d\rho}{\rho} + \frac{du}{u} + 2\frac{dr}{r} = 0 \tag{5}$$

For a rectangular fissure,

$$M = 2\rho u r L \tag{6}$$

and so

$$\frac{dp}{\rho} + \frac{du}{u} + \frac{dr}{r} + \frac{dL}{L} = 0 \tag{7}$$

The general expression for the bulk density of the magmatic fluid is

$$\frac{1}{\rho} = \frac{n}{\rho_g} + \frac{(1-n)}{\rho_l} \tag{8}$$

where n is the weight fraction of the mixture which consists of exsolved gas and ρ_g is the gas density. Under most conditions

the exsolved gas stays in good thermal contact with the liquid magma [*Wilson et al.*, 1980], and ρ_g is related to the pressure P by

$$P = \rho_g \frac{QT}{m} \quad \text{or} \quad \frac{dP}{P} = \frac{d\rho_g}{\rho_g} \tag{9}$$

where Q is the universal gas constant, m is the molecular weight of the gas, and T is the bulk temperature. If pressure changes occur very rapidly, the adiabatic relationship will be more accurate:

$$\frac{dP}{P} = \gamma \frac{d\rho_g}{\rho_g} \tag{10}$$

where γ is the ratio of the specific heats of the gas.

The equations (1), (8), and (5) or (7), together with the auxiliary definitions (2), (3), and (9) or (10), are adequate to describe most of the aspects of magma eruption. The total initial magma volatile content must be specified, and the solubility of the gas species must be known so that n may be defined as a function of pressure and temperature. Minor changes are needed if more than one gas species is exsolved. The above treatment neglects the possibility that the temperature T may decrease as the magma ascends owing to thermal losses at the walls or may increase owing to heat production by viscous dissipation or gas exsolution; any such temperature changes would cause viscosity changes in the magma. Fortunately, temperature changes would be progressive, being most apparent near the surface. We shall show below that over a very wide range of eruption conditions the motion of the erupting materials in the near-surface part of the system is turbulent; the Reynolds number is large and, as shown by (2) and (3), the friction factor becomes independent of the viscosity.

C. Role of Volatiles in Magma Rise

1. Gas-free case. Over the range of depths where no gas is exsolved from a magma, equation (8) shows that $\rho = \rho_l$, a constant and so $d\rho = 0$ and (5) and (7) are somewhat simplified. The small effect of the finite compressibility of the magmatic liquid is neglected. If we further assume that the conduit or fissure geometry does not change rapidly with depth we can put dr and $dL = 0$ (thus interpreting r and L as the average values applying to the system) which in turn implies $du = 0$ so that u is a constant, already defined as u_f. Inserting $du = 0$, $u = u_f$, and $\rho = \rho_l$ in (1) and substituting (2) and (3) for f leads to

$$\frac{K u_f^2}{4r} + \frac{A\eta u_f}{8r^2\rho_l} = g\frac{(\rho_h - \rho_l)}{\rho_l} \tag{11}$$

which is quadratic in u_f and inverts to

$$u_f = \frac{A\eta}{4K\rho_l r}\left\{\left[1 + \frac{64gr^3(\rho_h - \rho_l)K\rho_l}{A^2\eta^2}\right]^{1/2} - 1\right\} \tag{12}$$

This formula applies at any Reynolds number and is thus less cumbersome in use than the graphical results presented by *Shaw and Swanson* [1970] or the iterative solution method used by *Housley* [1978]. It will be useful to have the two approximations to this general formula which apply at high and low Reynolds numbers: at Reynolds numbers below about 10^2, (12) reduces to

$$u_{fL} = \frac{8gr^2(\rho_h - \rho_l)}{A\eta} \tag{13}$$

while at Reynolds numbers above about 3×10^4, we can put

$$u_{fH} = \left[\frac{4gr(\rho_h - \rho_l)}{K\rho_l}\right]^{1/2} \tag{14}$$

If the rising liquid is of Bingham rather than Newtonian type, the more general versions of (13) can be derived from *Johnson and Pollard* [1973] as

$$u_{fL} = \frac{8r^2}{A\eta}\left\{g(\rho_h - \rho_l) - B\frac{S_y}{r}\right\} \tag{15}$$

where, as before, $A = 64$ for a circular conduit and 24 for a fissure and now also $B = 2$ for a conduit and $B = (1 + (2r/L))$ for a fissure. Flow does not take place at all unless the value of the term in the bracket is positive.

It will be noted the above equations effectively assume that it is the magma density contrast which drives the motion of gas-free magma. For such a circumstance to apply exactly, there would have to be a steady deformation of the rocks around the magma reservoir to replace the volume of magma erupted. Prior to most eruptions there is probably a build-up of stress around a magma chamber due to injection of fresh magma from depth or tectonic adjustment (or gas exsolution if the chamber is at a shallow enough depth), and it is the release of this stress after the overlying rocks fail that initially drives the eruption and supplies the replacement volume [*Wadge*, 1980]. Numerical values given by *Wadge* [1980] show that the excess stresses typically have values which correspond to effective density contrasts of order 200 to 400 kg/m^3, only a factor of 2 greater than the contrasts between typical silicate solid/liquid densities.

2. General case. In the case where a finite amount of gas is present in the magmatic fluid the motion is dominated by the exsolution and subsequent expansion of the gas as the pressure decreases and is defined (to the extent that we initially assume good thermal contact between the magmatic liquid and the gas) by (1), (2), (3), and (5), or (7), (8), and (9). *Wilson et al.* [1980] have shown that these equations can be usefully reduced to

$$\left(1 - \frac{u^2}{u_c^2}\right)\frac{du}{dh} = -\left(\frac{u^2 f}{4r} + g\right)\frac{u}{u_c^2} - 2\frac{u}{r}\frac{dr}{dh} \tag{16}$$

and

$$\left(1 - \frac{u^2}{u_c^2}\right)\left(\frac{nQT}{mP} + \frac{(1-n)}{\rho_l}\right)\frac{dP}{dh} = 2\frac{u^2}{r}\frac{dr}{dh} + \left(g + \frac{u^2 f}{4r}\right) \tag{17}$$

in which the variable u_c, given by

$$u_c = \left(\frac{QT}{mn}\right)^{1/2}\left[n + \frac{(1-n)mP}{\rho_l QT}\right] \tag{18}$$

is introduced and identified as the effective speed of sound in the erupting fluid. This formula for u_c is somewhat simpler than those given by more exact derivations of the sound speed in multiphase fluids. Such formulae have been derived for various problems [*Hsieh and Plesset*, 1961; *Soo*, 1961, 1967; *Kliegel*, 1963; *Rudinger*, 1964; *Cole et al.*, 1970], including volcanic systems [*Kieffer*, 1977; *Pai et al.*, 1978]. Substitution of typical numerical values of ρ_l, Q, m, and T shows that for values of n up to about 0.06 (i.e., 6 wt %) and P up to several hundred bars (the ranges of interest), all these formulae produce values for u_c under isothermal conditions that lie within a few percent of those given by (18). Use of (10) instead of (9)

in deriving (16)–(18) shows that under conditions where the thermal exchanges in the gas are adiabatic the formulae are the same except that u_c is larger than that given by (18) by the factor $\sqrt{\gamma}$.

As *Housley* [1978] has pointed out, for erupting fluids in the vent region, pressure less than about 10 bars, (18) reduces adequately to $u_c = (nQT/m)^{1/2}$ and so for water at 1200 K as the exsolved volatile some values are $u_c = 160$ m/s for $n = 0.05$ (5 wt %), $u_c = 72$ m/s for $n = 0.01$, and $u_c = 23$ m/s for $n = 1000$ ppm. Other gas compositions lead to similar values because of the $m^{1/2}$ dependence. Since there is strong evidence that the eruption velocity in terrestrial plinian eruptions is commonly greater than 200 m/s [*Wilson*, 1976], the motion of the erupting mixture must be supersonic in such events.

Examination of (16) and (17) shows that there is no difficulty in allowing a subsonic to supersonic transition to occur in the conduit system, provided the conduit widens toward the surface with a wall slope numerically greater than the limiting value given by

$$\left(\frac{dr}{dh}\right)_L = \frac{rg}{2u_c^2} + \frac{f}{8} \tag{19}$$

As an example, assume that in a certain terrestrial eruption in which H_2O is the volatile released from a magma of liquid density $\rho_l = 3000$ kg/m^3 and temperature 1200 K, the erupting mixture rise speed becomes supersonic at a depth of about 300 m, where the pressure is 100 bars, the conduit radius is 5 m, and the exsolved gas weight fraction has reached $n = 0.02$. Then $u = u_c = 134$ m/s and $(dr/dh)_L = 1.4 \times 10^{-3} + (f/8)$. Equations (8) and (9) show that the bulk density of the erupting mixture is 1367 kg/m^3 under the stated conditions; the relative sizes of the terms in (8), which are proportional to the volumes of gas and liquid, respectively, shows that the gas occupies 76% of the total volume. This is close to the gas volume fraction at which magma disruption into a spray of scoria or pumice might be expected to occur [*Sparks*, 1978]. If we assume first that such disruption has not yet occurred, we must use the liquid viscosity in calculating the Reynolds number from (2): if we take $\eta = 10^2$ Pa s, we find $\mathrm{Re} = 1.83 \times 10^4$ and, using (3), $f = 0.0135$. Thus $f/8 = 1.69 \times 10^{-3}$ and $(dr/dh)_L = 3.1 \times 10^{-3}$. If, on the other hand, we assume that magma disruption has just occurred, the bulk viscosity of the gas/pyroclast mixture will essentially be equal to the gas viscosity [*Saffman*, 1967]: a typical value would be 2×10^{-5} Pa s. The Reynolds number would then be much larger, of order 10^{11}, and so (3) gives $f = 0.01$, leading to $(dr/dh)_L = 2.65 \times 10^{-3}$. Thus we find the value of $(dr/dh)_L$ needed to allow a supersonic transition to occur to be close to 3×10^{-3} in either case: this corresponds to a wall slope of only about 0.2° and is easily satisfied. Similar required wall slopes, of order 1°, are found for all other permutations of realistic values of the variables.

Equations (16)–(18) represent a convenient basis for numerical simulations of model eruptions. If it is assumed that the pressure is everywhere lithostatic, P and dP/dh are at once specified as a function of depth using the appropriate planetary gravity g and crustal density ρ_h. Values are selected for the molecular weight m of the desired volatile component and for the amount of that volatile component present in the magma at depth n_t (though a special treatment is required for the lunar case; see below). Provided the solubility n_d of the volatile is known as a function of pressure, n can be calculated at any depth. *Sparks* [1978] has shown that gas diffusion into nucleating bubbles will be sufficiently rapid that most magmas approaching the surface are only just supersaturated (by ~1 or 2 bars). We assume that rising magmas do always exsolve gas in this way as long as they remain coherent liquids. However, if the exsolved gas volume fraction exceeds 0.75 at some depth below the surface and disruption of the magma into pyroclasts and gas occurs, there will generally be a rapid increase in the upward velocity of the products (by a factor of order 10; see below). We assume that gas diffusion in the liquid phase will no longer be able to keep pace with the falling pressure under these conditions and so terminate gas exsolution if magma disruption occurs.

Numerical solutions are normally started from the level where $n = 0$, since the motion below that level is fixed by (12), which gives u_f, the constant value of u, in terms of the chosen values of ρ_h, ρ_l, g, η, and r. Equation (18) is used to find u_c, (17) gives dr/dh, and finally, (16) gives du/dh. A simple integration scheme (with automatic adjustments of the vertical height increment to maintain accuracy) allows the increments in r and u to be found. The local values of bulk density ρ are obtained from (8). Values for Re and hence f (equations (2) and (3)) are calculated using the magmatic liquid viscosity at first; the ratio of the terms on the right-hand side of (8) is used to keep track of the fractional volume of the erupting mixture occupied by gas. When (and if) this fraction rises to 0.75, it is assumed that the magma disrupts rapidly into scoriaceous or pumiceous droplets and released gas: the gas viscosity then replaces the liquid vicosity in finding the Reynolds number. For mathematical convenience this transition is idealized as being abrupt, whereas in real systems it must occur over a finite vertical distance. However, the simplification is of little consequence, since in almost all cases (as in the example above), when disruption occurs, the term (A/Re) in (3) has already become comparable with or smaller than K; thus the sudden large increase in Re due to the change from using a liquid viscosity to using a much smaller gas viscosity produces only a small change in f and hence the rate of change of r and u with depth.

It is emphasized that the above assumption of P varying lithostatically with depth is not essential. The extreme alternative is to use (12) as before to fix the motion below the level at which n becomes nonzero but afterward to specify r instead of P as a function of h. The corresponding integration that gives u and P as a function of depth. Of course, if $r(h)$ is chosen to vary very rapidly, then pressure profiles which rapidly cease to be even vaguely lithostatic can be generated. As we argued above, such circumstances do not, presumably, occur commonly in real volcanic systems, since they lead to very large stresses across the conduit walls. Nonetheless, this alternative mode of solution of the equations is useful in illustrating the early stages of an eruption (see later) or in exploring the consequences of episodes of sudden conduit widening (by erosion of wall rock) or narrowing (by tectonic adjustments) which might occur. *Wilson et al.* [1980] give some examples of the latter processes.

III. Constraints on Maximum and Minimum Rise Rates of Magmas

A. *Minimum Rise Rates*

We can now summarize formulae for the effects of cooling and yield strength on magma rise and deduce values for the minimum conduit radii that must be considered in later sec-

TABLE 1. Values of Minimum Conduit Radius Allowing Motion r_{cy} as a Function of Yield Strength s_y and Planetary Gravity g for a Magma Whose Rise is Limited by Yield Strength

Planet	g, m/s^2	s_y, N/m^2			
		1, mm	10^2, m	10^4, m	10^6, km
Earth	9.81	1.0	0.10	10	1.0
Mars	3.74	2.7	0.27	27	2.7
Moon	1.62	6.2	0.62	62	6.2

Values given are for a density contrast $(\rho_h - \rho_l) = 200$ kg/m^3.

tions. The fundamental constraint is the possible existence of a yield strength large enough to counterbalance the driving density contrast: if we set $u = 0$ in (15), we find that for flow to take place, r must be greater than a critical value r_{cy} given by

$$r_{cy} = \frac{Bs_y}{g(\rho_h - \rho_l)} \tag{20}$$

Values of s_y may be of order 10^2 N/m^2 for long lunar basaltic flows after they leave the vent and can be as high as 10^6 N/m^2 for terrestrial dacite flows on the surface [*Hulme and Fielder*, 1977]. Table 1 shows the variations of r_{cy} with s_y for $(\rho_h - \rho_l) = 200$ kg/m^3 for the earth ($g = 9.81$ m/s^2), moon ($g = 1.62$ m/s^2), and Mars ($g = 3.74$ m/s^2), using $B = 2$ for a circular conduit.

Clearly, very large values of conduit radius or fissure width (in excess of 1 km) would be needed to allow terrestrial dacites to reach the surface if their yield strengths at depth were as high as their yield strengths on the surface. This observation lends support to the suggestions of *Sparks and Pinkerton* [1978] that an increase commonly occurs in both the viscosity and yield strength of magmas as they are degassed on nearing the surface.

Fedotov [1978] has shown that if a magma is to avoid excessive cooling during its rise from some depth H, its velocity must be greater than a critical value u_{ct} given by

$$u_{ct} = H/\tau \tag{21}$$

where τ is a characteristic cooling time given by *Jaeger* [1964] as

$$\tau = r^2/4\chi\beta^2 \tag{22}$$

in which β is a dimensionless number and χ is the thermal diffusivity, typically about 7×10^{-7} m^2/s. The value to be adopted for β depends on the amount of cooling allowed. *Fedotov* [1978] assumes that the initial and final temperatures to be used are the liquidus and solidus, respectively, in which case $\beta = 0.65$. However, the common presence of phenocrysts in erupted magmas implies that initial magma temperatures are generally subliquidus, but to offset this fact we note that gas exsolution is commonly exothermic [*Burnham and Davis*, 1974] and can cause heating of at least 10 K per wt% of water exsolved, and we conclude that the use of β 0.65 should provide a better than order of magnitude estimate of the required amount of cooling. Combining (21) and (22), we have

$$u_{ct} = ZH/r^2 \tag{23}$$

with $Z = 4\chi\beta^2 = 1.25 \times 10^{-6}$ m^2/s. If we assume for the moment that a magma rising at a speed just equal to u_{ct} is flowing in a laminar fashion and has a negligible yield strength, we can equate (23) to (13) to find a relationship for the value of r, say r_{ct}, which just permits magma motion to occur:

$$r_{ct} = \left[\frac{ZHA\eta}{8g(\rho_h - \rho_l)}\right]^{1/4} \tag{24}$$

Because of the fourth root dependence, r_{ct} is quite insensitive to the exact value adopted for Z, $(\rho_h - \rho_l)$, or even g: the sixfold range of gravity between the earth and moon, which brackets the range for the terrestrial planets, leads to a variation in r_{ct} by a factor of only 1.57. For all possible permutations of H in the range 10 m to 100 km and η in the range 1 to 10^4 Pa s, r_{ct} varies only from 15 mm to 1.5 m; furthermore, in every case the Reynolds number is sufficiently small that flow is in the laminar regime, and the use of (13) in the above treatment is justified. Table 2 shows some values of r_{ct}, u_{ct}, and the corresponding Reynolds number Re_{ct} for flow in a circular conduit ($A = 64$) for $(\rho_h - \rho_l) = 200$ kg/m^3 and $g = 9.81$ m/s^2. In a corresponding lunar case, values of r_{ct} would be 1.57 times smaller, values of u_{ct} would be smaller by a factor of 2.4, and values of Re_{ct} would be larger by a factor of 1.57.

It is conventional to assume that the rise of magmas is indeed limited by cooling and hence, in terms of rheology, by viscosity rather than yield strength. The relative importance of these two properties can be quantified. If the yield strength is to be less important than the viscosity in limiting the magma rise, we must have $r_{ct} \gg r_{cy}$; substituting from (24) and (20) and rearranging, we find the requirement

$$s_y \ll \left[\frac{ZHA\eta g^3(\rho_h - \rho_l)^3}{8B^4}\right]^{1/4} \tag{25}$$

The fourth root dependence of s_y on H and η means that limiting values for s_y can be found quite accurately even for a wide range of values of depth of magma origin and magma viscosity. If we use $(\rho_h - \rho_l) = 200$ kg/m^3, $H = 10$ km, a circular conduit, and $g = 9.81$ m/s^2 for the earth, we have the following limiting values: $\eta = 10$ Pa s, $s_y \ll 150$ N/m^2; $\eta = 10^3$ Pa s, $s_y \ll 470$ N/m^2; $\eta = 10^5$ Pa s, $s_y \ll 1480$ N/m^2. In each case the yield strength must be less than the value indicated (by about a factor of 10) before its effect on limiting the magma rise can be neglected. Under what may have been typical lunar conditions (see below) with $(\rho_h - \rho_l) = 200$ kg/m^3, $H = 100$ km, and $g = 1.62$ m/s^2, we have the following combinations: $\eta = 10$ Pa s, $s_y \ll 70$ N/m^2; $\eta = 10^3$ Pa s, $s_y \ll 220$ N/m^2; $\eta = 10^5$ Pa s, $s_y \ll 700$ N/m^2.

TABLE 2. Values of Minimum Conduit Radius r_{ct}, Minimum Rise Speed u_{ct}, and Corresponding Reynolds Number Re_{ct}, as a Function of Magma Viscosity η and Depth of Magma Source H for Cooling Limited Terrestrial Eruptions of Magma With Zero Yield Strength

H =	Values of r_{ct}, m			Values of u_{ct}, mm/s			Values of Re_{ct}		
η, Pa s	10 m	1 km	100 km	10 m	1 km	100 km	10 m	1 km	100 km
1	0.015	0.047	0.15	55	559	5550	5	160	5×10^3
10^2	0.047	0.015	0.47	5.6	55	559	1.6×10^{-2}	0.6	16
10^4	0.15	0.47	1.50	0.55	5.6	55	5×10^{-5}	1.6×10^{-3}	5×10^{-2}
10^6	0.47	1.5	4.73	0.056	0.55	5.6	1.6×10^{-7}	5×10^{-6}	1.6×10^{-4}

TABLE 3. Values of Mass Eruption Rate M and Rise Velocity at Depth u_f in a Circular Conduit of Radius r for a Terrestrial Basalt With Viscosity 300 Pa s and Density 2800 kg/m^3 Rising Through a Crust With Density 3000 kg/m^3

r, m	u_f, m/s	M, kg/s
0.2	0.033	11.5
0.3	0.074	58.2
0.5	0.20	449
0.7	0.40	1.7×10^3
1	0.8	7.2×10^3
3	6.9	5.5×10^5
10	38.5	3.4×10^7
30	86.2	6.8×10^8

The above results can be used as follows. For any chosen magma composition and temperature at depth the viscosity and yield strength must be estimated. Interpolation among the above pairs of values of viscosity and yield strength allows a decision to be made as to which factor dominates in limiting the magma rise. If yield strength dominates, Table 1 can be used to find the minimum conduit or fissure size which permits an eruption to occur. If viscosity-controlled cooling dominates, Table 2 gives the minimum conduit dimension.

There is an appreciable body of laboratory and field data on magma rheology [*Shaw et al.*, 1968; *Shaw*, 1969; *Murase and McBirney*, 1970, 1973; *Kushiro et al.*, 1976; *Pinkerton and Sparks*, 1978] but most of these data refer to viscosity rather than yield strength. While *Shaw* [1972] and *Bottinga and Weill* [1972] have presented empirical methods of estimating magma viscosity as a function of composition and temperature, no corresponding reliable method of estimating yield strength yet exists (H. Pinkerton, personal communication, 1979). The upward transport of relatively large xenoliths in magmas which may not have had a high rise velocity suggests the existence in such magmas of an appreciable yield strength at depth [*Sparks et al.*, 1977]. Certainly, magmas with a wide range of composition exhibit appreciable yield strengths after they have been erupted as lavas [*Shaw et al.*, 1968; *Hulme and Fielder*, 1977; *Pinkerton and Sparks*, 1978], but it is not safe to use this observation to infer a similar yield strength at depth in the conduit system, since such liquids may acquire at least part of their yield strength as a result of degassing which occurs in the vent [*Sparks and Pinkerton*, 1978]. We conclude that there are currently insufficient data on yield strength values to allow the above analysis to be carried out. Fortunately, if we assume that magmas are cooling-limited, we obtain a realistic estimate of the minimum conduit or fissure width required for an eruption. It is always the larger of r_{ct} and r_{cy} which must be exceeded for flow to the surface to occur, and comparison of Tables 1 and 2 shows that while r_{cy} can realistically go to zero as s_y goes to zero in a magma at a temperature approaching the liquidus, r_{ct} can never do so, since all magmas, however hot, must have a finite viscosity. If we assume that terrestrial basalts commonly erupt from a minimum depth of 5 km and have minimum viscosities of 10^2 Pa s, we should expect a minimum conduit radius of about 0.22 m, which is consistent with the observed range of widths of terrestrial dikes [*Fedotov*, 1978]. The corresponding minimum rise velocity would then be 0.12 m/s for a density contrast of 200 kg/m^3. For a terrestrial rhyolite with $\eta = 10^4$ Pa s and the same depth of origin and density contrast, the minimum conduit radius would be 0.7 m and the minimum rise speed 12.5 mm/s. The corresponding calculations for lunar basalts, for which we may take a minimum viscosity of 10 Pa s and a minimum depth of origin of 60 km [*Kesson and Lindsley*, 1976; *Papike et al.*, 1976], give a minimum conduit radius of 0.37 m and a minimum rise speed of 0.55 m/s.

There is an interesting property of the cooling limitation process which can be illustrated by evaluating the minimum mass eruption rate for a cooling-limited eruption. If we insert u_{ct} from (23) for u in the equation for the mass eruption rate M through a circular conduit, given in (5), we see that the minimum mass flow rate M_{ct} is

$$M_{ct} = \pi \rho_l Z H \tag{26}$$

which is independent of the magma viscosity and the planetary gravity and depends mainly on the depth of the magma source H. If we assume, as above, that magmas involved in most terrestrial eruptions are derived from depths of no less than 5 km, we find $M_{ct} \approx 60$ kg/s; similarly, if the lunar mare basalts erupted from depths of not less than 60 km, their eruption rates could not have been less than about 700 kg/s.

An analogous treatment exists for the case of an eruption through an elongate conduit. If (7) is used for the mass rise rate M, we find

$$\frac{M_{ct}}{L} = 2\rho_l \left[\frac{8g(\rho_h - \rho_l) Z^3 H^3}{A\eta} \right]^{1/4} \tag{27}$$

Using $\eta = 300$ Pa s as typical for terrestrial basalts and a minimum depth of origin of 5 km as before, we have a minimum eruption rate of 160 kg/s per meter length of fissure. The corresponding lunar value is about 1600 kg s^{-1} m^{-1}.

All of the above minimum mass eruption rates have been calculated for the case where a magma cools from its liquidus to its solidus temperature during vertical ascent through a conduit or fissure of the simplest possible, and hence most favorable, geometry. Since lower initial temperatures are quite possible and real conduit systems almost certainly have more complex shapes and hence offer more resistance to magma motion than those used in the calculations, mass eruption rates substantially greater than the values given above are probably needed if appreciable eruptions are to occur other than from reservoirs at very shallow depths. In confirmation of this point we note that a recent survey (J. L. Whitford-Stark, manuscript in preparation, 1979) shows that the majority of basaltic mass eruption rates are greater than 10^4 kg/s, an order of magnitude greater than the minimum value calculated above for a circular vent.

B. *Maximum Rise Rates*

The maximum rate of rise of a magma through a fissure or conduit is dictated for any given set of values of magma yield

TABLE 4. Values of Mass Eruption Rate M and Rise Velocity u_f in a Circular Conduit of Radius r for a Lunar Basalt With Viscosity 10 Pa s and Density 2800 kg/m^3 Rising Through a Crust With Density 3000 kg/m^3

r, m	u_f, m/s	M, kg/s
0.3	0.36	288
0.6	1.45	4.6×10^3
1	3.4	3.0×10^4
3	10.5	8.3×10^5
10	21.6	1.9×10^7
30	37.9	3.0×10^8
100	68	6.1×10^9

TABLE 5. Values of Mass Eruption Rate per Unit Length of Fissure M/L and Magma Rise Velocity at Depth u_f in a Fissure of Half Width r for a Terrestrial Basalt With Viscosity 300 Pa s and Density 2800 kg/m^3

r, m	u_f, m/s	M/L, kg s^{-1} m^{-1}
0.2	0.087	97.7
0.3	0.2	330
0.6	0.79	2.6×10^3
1	2.1	1.2×10^4
3	14.6	2.5×10^5
10	47	2.6×10^6
30	90	1.5×10^7

strength, viscosity, and density, crustal density, and planetary gravity by the maximum value during the eruption of the average width of the pathway through relationships like (20) or (24). As noted earlier, at the onset of an eruption the width is probably determined by the amount of regional stress relieved by the opening of a fracture, while wall erosion during a prolonged eruption could significantly enlarge the width. We do not attempt to quantify these processes but note that mass eruption rates are commonly less than about 3×10^6 kg/s in basaltic eruptions on earth and are inferred to have been up to 10^9 kg/s for some lunar mare basalt flows (J. L. Whitford-Stark, manuscript in preparation, 1979).

If (5) and (12) are combined to give M as a function of r for a circular conduit, it is readily shown that for typical terrestrial basalt eruption conditions a mass eruption rate of 3×10^6 kg/s implies a conduit radius of about 5 m. Table 3 shows some values of u_f and M corresponding to several values of r for these conditions. The corresponding results for lunar eruption conditions are shown in Table 4, where a mass eruption rate of 10^9 kg/s would require a conduit radius of 50 m.

It is unlikely that large-scale basaltic eruptions take place through a single, circular conduit system. All such eruptions on earth in historic time have involved fissure sources, and at least some lunar basaltic vents appear to be elongate [*Schultz*, 1976]. Since it is the width rather than the length of an elongate fissure which controls the magma rise velocity, the output from such a source must be specified as a mass flow rate per unit length of the fissure. Unfortunately, even detailed descriptions of observed eruptions rarely include the exact geometry of the vent or the lengths of fissure segments actually delivering magma to the surface. From measurements given by *Thorarinsson and Sigvaldason* [1962] for the 1961 basaltic fissure eruption in Askja we deduce a maximum eruption rate of 0.8 to 1.0×10^4 kg s^{-1} m^{-1}, while from *Thorarinsson*'s [1969] summary of the great 1783 Lakagigar eruption we obtain a value of at least 1.5×10^3 kg s^{-1} m^{-1}. *Swanson et al.* [1975] estimated an eruption rate of about 3×10^4 kg s^{-1} m^{-1} for the Yakima member of the Columbia River basalt series.

If (7) and (9) are combined to give M as a function of r and L we find

$$\frac{M}{L} = \frac{A\eta}{2K}\left\{\left[1 + \frac{64gr^3(\rho_k - \rho_l)K\rho_l}{A^2\eta^2}\right]^{1/2} - 1\right\} \quad (28)$$

with $A = 24$ for a fissure. Table 5 shows some values of M/L and u_f corresponding to a range of values of fissure half width r for terrestrial eruptions. Values of M/L up to 3×10^4 kg s^{-1} m^{-1} imply fissure widths at depth up to about 4 m. The corresponding lunar calculations shown in Table 6 indicate that this eruption rate would require a fissure width of about 2 m.

The results of the above calculations can be summarized as follows. If basaltic eruptions take place through elongate fissures, then such fissures must commonly have widths of at least 0.1 m if the magma is to avoid cooling as it rises (see Table 2); also, the fissures could accommodate the largest effusion rates inferred for terrestrial flood basalt eruptions if they were typically 4 m wide on earth or 2 m wide on the moon. Equation (28) shows that a 4.6-fold increase in width would permit a 10-fold increase in effusion rate. If magmas possess a yield strength greater than about 10^3 N/m^2, then their rise will be limited by the yield strength rather than by cooling, and fissure widths will need to be much wider than 1 m to permit eruptions to occur; see Table 1. Finally, if eruptions occur through central conduits rather than elongate fissures, then conduit radii up to several tens of meters will be needed to accommodate the highest expected eruption rates; see Tables 3 and 4.

IV. Ascent and Emplacement of Basaltic Magmas on Earth

A. *Volatiles: Compositions and Solubilities*

We assume that H_2O and CO_2 are the most common volatiles in terrestrial magmas [e.g., *Holloway*, 1976]. *Mysen* [1977] has summarized the available data on solubility of H_2O in liquids of common mineral compositions and in real magmas. The solubility varies appreciably with the composition of the host liquid, being generally greater in rhyolitic liquids than in basaltic liquids at a given temperature and pressure for pressures up to at least 10 kbar. There is a strong dependence on pressure for a fixed temperature and composition and a weak dependence on temperature for a fixed composition and pressure. We neglect the temperature dependence (which will be justifiable retrospectively) and find the following functions to be convenient approximations to the experimental data: if n_d is the solubility in wt % and P_b is the total pressure in bars, then for water in rhyolite,

$$n_d = 0.13P_b^{0.5} \quad (29)$$

while for water in basalt,

$$n_d = 0.0215P_b^{0.7} \quad (30)$$

These rather simple functions are quite adequate for our purposes, which only require us to be able to calculate the amount of volatile exsolved from a given magma with a chosen initial volatile content at depth as the magma rises, and the total pressure decreases to values much less than about 1 kbar.

The solubility of CO_2, like that of water, is a function mainly of magma composition and total pressure. At pres-

TABLE 6. Values of Mass Eruption Rate per Unit Length of Fissure M/L and Magma Rise Velocity at Depth u_f in a Fissure of Half Width r for a Lunar Basalt With Viscosity 10 Pa s and Density 2800 kg/m^3

r, m	u_f, m/s	M/L, kg s^{-1} m^{-1}
0.1	0.11	60.5
0.2	0.43	484
0.3	0.9	1.5×10^3
1	5.0	2.8×10^4
3	11.1	1.9×10^5
10	21.3	1.9×10^6
30	37.2	6.2×10^6

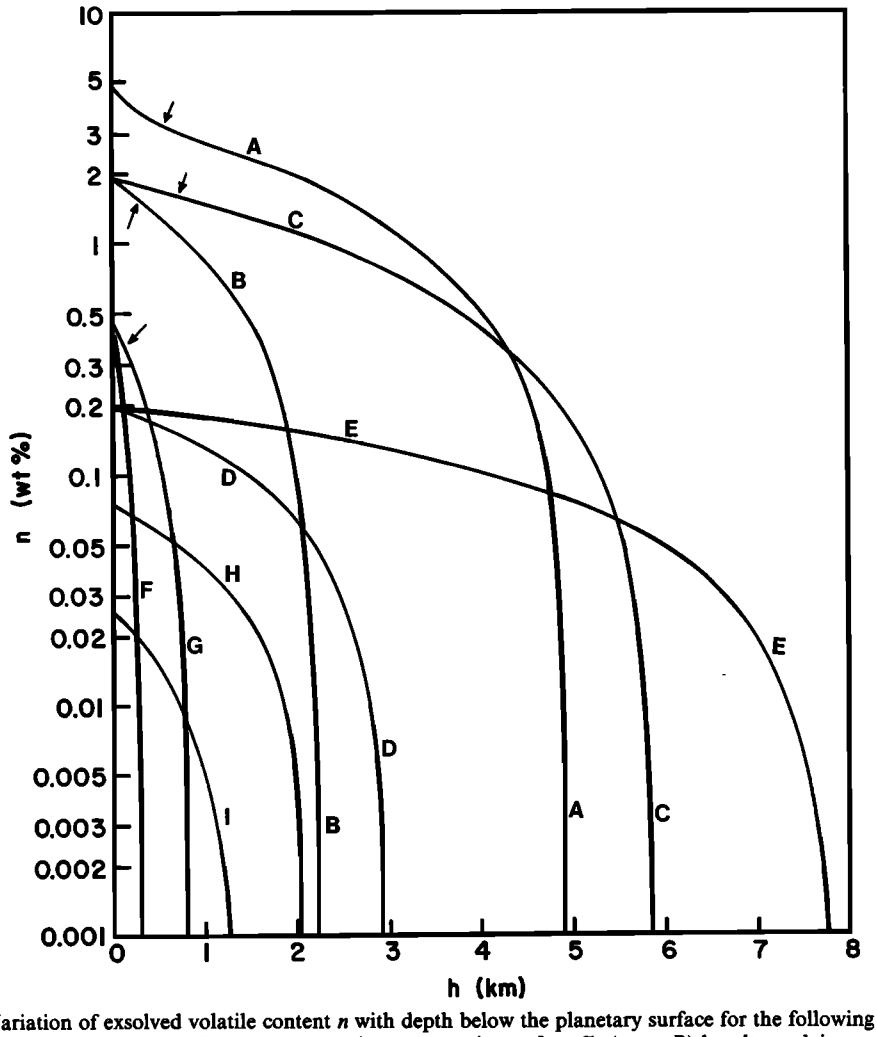

Fig. 2. Variation of exsolved volatile content n with depth below the planetary surface for the following cases: (curve A) rhyolite exsolving water on earth, water content in source region = 5 wt %; (curve B) basalt exsolving water on earth, water content in source region = 2 wt %; (curve C) as for curve B but on Mars; (curve D) any magma on earth exsolving CO_2, CO_2 content in source region = 0.2 wt %; (curve E) as for curve D but on Mars; (curve F) basalt exsolving water on earth, water content in source region = 0.5 wt %; (curve G) as for curve F but on Mars; (curve H) lunar basalt exsolving CO, final CO content in erupting magma = 750 ppm by weight; (curve I) as for curve H but final CO content = 250 ppm.

sures below about 10 kbar the best approximation to all available data referenced in *Mysen* [1977] is

$$n_d = 0.00023 P_b \tag{31}$$

with n_d in wt % and P_b in bars, as before.

When simulating eruptions, the scheme outlined in section II*B* is used for calculating n as a function of depth: the volatile phase (H_2O or CO_2) is assumed to exsolve progressively so that the magma is always just saturated. Figure 2 shows a number of examples of the variation of n with depth. Since there is strong evidence for the presence of large quantities of subsurface water on Mars [*Mutch et al.*, 1976] and the main component of the atmosphere is CO_2, there seems to be no reason to assume that any gases other than these two may have been involved in martian volcanism, and Figure 2 shows examples for both planets, illustrating the effects of the differing gravities and surface pressures. Where space permits in Figure 2, an arrow is inserted to show the combination of depth and released gas content at which the gas volume fraction in the magma reaches 0.75 and magma disruption is expected to occur. Such disruption is expected to occur for every curve in the figure, albeit very close to the surface in some cases, unless the eruption occurs through a sufficiently narrow conduit that the magma rise speed is much less than the rise speed of individual gas bubbles in the magma. Under these conditions, bubble coalescence can occur, and strombolian explosive activity can develop. This process is considered in more detail later. Magma disruption can be guaranteed not to occur only if the magma volatile content is so low that the exsolved gas volume fraction does not reach 0.75 even when the magma emerges into the planetary atmosphere. This condition corresponds to an exsolved water content less than 0.058 wt % on earth and less than 4 ppm by weight on Mars or to a CO_2 content less than 0.14 wt % on earth and less than 10 ppm on Mars.

B. The Opening Phase of an Eruption

In order to illustrate some of the effects of conduit shape on the eruption conditions, especially in the opening stages of an eruption, we have compared, in Figures 3–5, the results of requiring the pressure in the erupting fluid to be everywhere lithostatic (case A) with the results of requiring the conduit radius to take on each of a series of specified variations with depth (cases B–G). We show the rise velocity u (Figure 3), to-

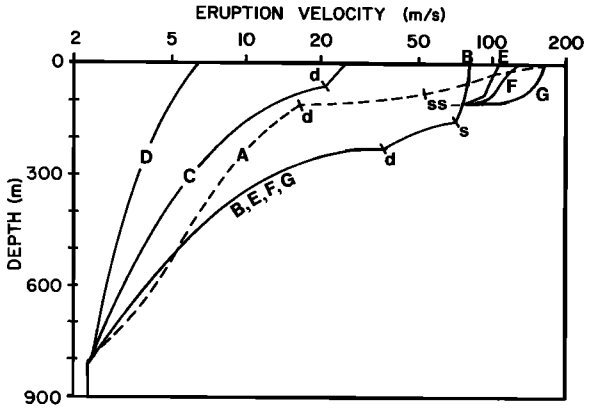

Fig. 3. Variation of upward velocity of magma with depth for terrestrial eruptions in which the magma has density 2800 kg/m^3, viscosity 10^3 Pa s, and total water content 1 wt % and rises in a circular conduit at a rate of 2×10^5 kg/s. Curve A is for the case in which the pressure is lithostatic at all depths; curves B–G refer to the imposed conduit shapes shown in Figure 5. Near points labeled d, magma disrupts into gas and pyroclasts as the fractional gas volume reaches 0.76. Flow becomes sonic at the point labeled s and supersonic at the point labeled ss.

tal pressure, P (Figure 4), and conduit radius r (Figure 5) for a magma of density 2800 kg/m^3, viscosity 10^3 Pa s, and total water content 1 wt % rising in a circular conduit through a crust with density 3000 kg/m^3 at a mass flow rate of 2×10^5 kg/s. Below the level where gas begins to exsolve (816 m) the pressure gradient is assumed to be close to lithostatic, and (12) and (5) show that the rise velocity is 2.36 m/s through a conduit of average radius 3.1 m.

If the pressure is everywhere lithostatic, so that there are no stresses across the conduit walls, the rise velocity increases monotonically toward the surface (case A, Figure 3). The volume fraction occupied by growing gas bubbles reaches 0.75 at a depth of 108 m, and magma disruption is assumed to occur at this depth. The lowered effective viscosity results in an acceleration until the gas/pyroclast mixture makes a subsonic/supersonic transition at a depth of 53 m to reach the surface with an exit velocity u_e of 160 m/s. This velocity applies to the gas phase and all clasts small enough to have a negligible terminal velocity in the gas—in this case those smaller than about 2-cm diameter: the motion of particles larger than this size in the vent region will be quite complex as the surrounding gas velocity and density change with depth. The variation of conduit radius with depth required to permit the pressure to be lithostatic everywhere (Figure 5, curve A) appears rather irregular due to the exaggerated horizontal scale; however, wall slopes are nowhere greater than 1° below a depth of 20 m and reach only 25° within the last meter of the surface. The

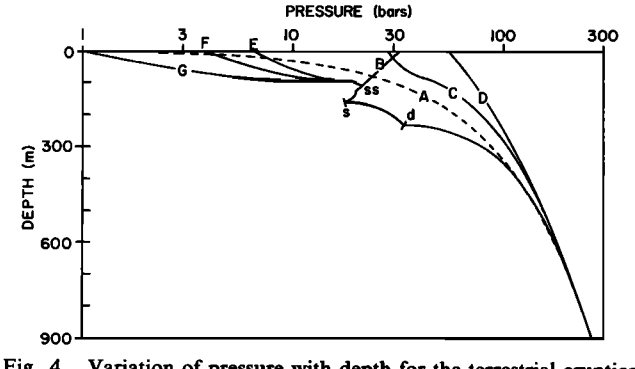

Fig. 4. Variation of pressure with depth for the terrestrial eruption models defined in the caption to Figure 3.

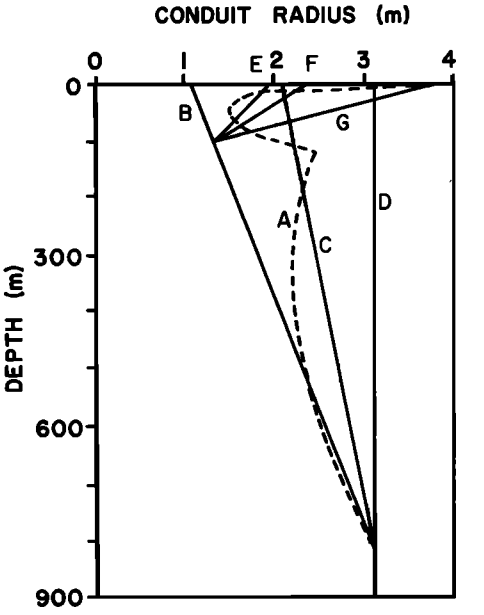

Fig. 5. Variation of conduit radius with depth for the terrestrial eruption models defined in the caption to Figure 3.

main feature of the required conduit shape is the slight narrowing toward the surface over the depth range 100 to 800 m. This shape is consistent with the observation that opening fissures propagate upward toward the surface rather than downward. Models B, C, and D show that the result of a progressive change during the onset of an eruption from a conduit which narrows rapidly toward the surface (B) to one which is straight-sided (D) is to decrease the (subsonic) exit velocity (Figure 3) and raise the near-surface and exit pressures above atmospheric. In models B and C, magma disruption into released gas and pyroclasts occurs at some point below the surface; in model D, disruption would occur immediately above the vent, as the 50-bar pressure was relieved.

In an upward narrowing conduit (model B) the erupting mixture's rise velocity can reach the local sonic velocity (at depth 160 m in this case (Figure 3)) but cannot make a supersonic transition due to the geometry (see equation (19)). However, the effect of the resulting excess pressures (of order tens of bars) over the last few tens of meters near the surface (model B, Figure 4) should be to blow out the near-surface rock and accumulating eruption products in the vent into a flared shape (models E, F, and G, Figure 5) which will permit the supersonic transition to occur and lead to exit pressures close to atmospheric (Figure 4) and high exit velocities (Figure 3).

These early adjustments should occur very rapidly once magma approaches the surface. During the period when the exit pressure is greater than atmospheric, violent expansion of the gas phase should occur just above the vent, accelerating the eruption products to much higher speed. Because of the short time scale of this expansion it is probably best to assume that the process would occur adiabatically rather than isothermally. A good approximation to the solution to (1) for such conditions [*Wilson*, 1980; *Self et al.*, 1979] is obtained by neglecting the potential energy and friction terms (the last two terms on the right-hand side) and using (8) and (10) to eliminate ρ and ρ_g in terms of P. On integrating:

$$\left(\frac{\gamma}{\gamma-1}\right)\left(\frac{nQT}{m}\right)\left[1-\left(\frac{P_a}{P_e}\right)^{(\gamma-1)/(\gamma)}\right] = 0.5(u_f^2 - u_e^2) \quad (32)$$

where P_a is atmospheric pressure, P_e and u_e are the pressure and upward velocity in the vent at ground level, and u_f is the final velocity reached by the products after the sudden expansion. Using the example of model B, we have $P_e = 31.5$ bars (Figure 4) and $u_e = 81$ m/s (Figure 3). From our numerical solutions we find the exsolved water content of the mixture in the vent in this case to be 0.75 wt %. Using these values and $\gamma \approx 1.26$, we have $u_f = 156.8$ m/s. This value is very close to that found for model A (160.0 m/s) in which the pressure was assumed to be lithostatic at all depths. Thus the delay in final gas expansion caused by the unfavorable vent geometry does not drastically change the expected final eruption velocity.

The mechanism of the rapid expansion to atmospheric pressure consists initially, in the terrestrial case, of the horizontal propagation of an expansion wave into the mixture of gas and clasts rising through the vent. The speed of the wave front will be the same as the speed of sound in the unexpanded mixture, u_c, given by (18), and so the time required for the wave to travel from the edge to the center of the emerging jet will be equal to the jet radius divided by the sound speed. Using the numerical values for model B again, we find $u_c = 81$ m/s. As expected, this value is equal to u_e (Figure 3): in model B the eruption velocity is limited to be equal to the sound speed, since the vent geometry prevents a supersonic transition. The emerging jet radius is 1.1 m (Figure 5), and so the time for passage of the front of the expansion wave is 14 ms. Decompression is not completely accomplished by the passage of the expansion wave, since the radial outward flow of gas behind the wave must cease eventually once the pressure in the rising gas is everywhere atmospheric. These further adjustments may be thought of as the consequence of the passage of further waves across the radius of the jet. The total time scale required will be a few times longer than the 14 ms calculated above: perhaps 50 ms but certainly not greater than 0.1 s. Since the vertical velocity component increases from 81 to 160 m/s during this period, the mean upward velocity is close to 120 m/s, and the eruption products will rise no more than 12 m in 0.1 s. Thus then rapid expansion of the erupted gas to atmospheric pressure should occur within 10 m of the ground level in the case of model B.

C. *The Main Phase of a Steady Eruption*

The above example shows that an adequate approximation to the final vertical eruption velocity of gas and small clasts is obtained by making the assumption that the pressure in the conduit system is lithostatic at all depths. Using this condition, we have computed velocities and implied conduit or fissure profiles for wide ranges of values of mass eruption rate, M, magma viscosity η, and exsolved gas content n to cover all combinations for terrestrial basalts.

1. Vent geometry. Figure 6*a* shows the variations of circular vent radius with mass eruption rate for $\eta = 300$ Pa s and three values of the released water content. The vent radii change by less than 10% if the magma viscosity is increased or decreased by a factor of 10. The dashed line represents the conduit radius below the level where gas is first exsolved; thus a net upward widening of the conduit is required for all mass eruption rates greater than about 3×10^4 kg/s if the exit pressure is to be exactly atmospheric, while a net narrowing is needed at very low effusion rates. The equivalent results for eruptions through fissures are shown in Figure 6*b*, and a similar pattern is seen. We stress that these vent sizes only apply when the pressure gradient near the surface is exactly lithostatic/hydrostatic. In cases where the topography near the vent allows a lava lake of appreciable depth to form, the transition from mainly upward to mainly lateral flow will occur in a complex manner, and the apparent vent shape may be quite different from that shown in Figure 6 for the corresponding mass flow rate and gas content. In general, it will be true that the higher is the vertical eruption velocity in the vent and hence the higher the lava fountain over the vent, the more nearly will the shape of the base of the fountain reflect the shape of the vent as calculated above.

2. Eruption velocities and fountain heights. Figure 7*a* shows the relationship between the vertical velocity u_e of the eruption products (gas and small pyroclasts), leaving a circular vent and the released gas content n for several values of the mass eruption rate of a magma with viscosity, $\eta = 300$ Pa s; Figure 7*b* is the corresponding diagram for a fissure. Also indicated in Figures 7*a* and *b* are the heights to which fire fountains should be projected. The heights are taken to be equal to $u_e^2/2g$, so that air resistance to the motion of the ejecta in the center of the fountain is neglected. This is probably a good approximation since for a steady or nearly steady fountain most of the coarse ejecta fall back to the ground in an envelope around the central core, thus protecting material in the center from interaction with the surrounding atmosphere. The structure is essentially a 'collapsed eruption column' of the type analyzed by *Sparks et al.* [1978]. Finally, the right-hand sides of Figures 7*a* and 7*b* show the total gas contents n_t before the onset of gas release which correspond to the exsolved gas contents on the left-hand axes.

Figure 7 represents probably the most useful result of the calculations for terrestrial basalts. If an eruption is sufficiently well documented that the mass eruption rate (for a central source) or the mass eruption rate per unit length of fissure (for an elongate source) and the fire fountain height can be determined at the same time (or over the same short period), then the released gas content can be deduced. Figure 7 is plotted for a magma viscosity of 300 Pa s. It may be used for other magma viscosities as follows. An initial approximation to the released gas content n_{app} is read off the figure by using the observed fountain height and appropriate eruption rate. For a central source (Figure 7*a*), Table 7 is used to find (by interpolation) the value of the dimensionless quantity K which applies for the relevant pair of values of M and n_{app}. A final approximation to the released gas content n_{final} is then found from

$$n_{final} = n_{app} K^{[0.91 \ln(\eta/300)]} \tag{33}$$

where η is the observed magma viscosity expressed in Pa s. For a fissure source (Figure 7*b*), Table 8 is used in an equivalent way. This approximate correction procedure cannot be relied upon for viscosities greater than 3000 Pa s or less than 30 Pa s, but this range should cover the vast majority of terrestrial basaltic eruptions.

3. Comparisons with observations. Although there are few eruptions for which active fissure lengths, effusion rates, and magma viscosities have been simultaneously recorded, three examples can be given. Near the beginning of the 1973 Heimaey eruption the effusion rate was at least 100 m^3/s, i.e., 3×10^5 kg/s, and fire fountains rose 50 to 100 m [*Thorarinsson et al.*, 1973]. The total length of the fissure was 1500 m, but a photograph shows that only about one third of the length was producing substantial fountains. Thus the required output rate is about 600 kg s^{-1} m^{-1}. No values are given for the viscosity; however, Table 8 shows that K is so close to unity at low values of M/L that the exact value of the viscosity in (33)

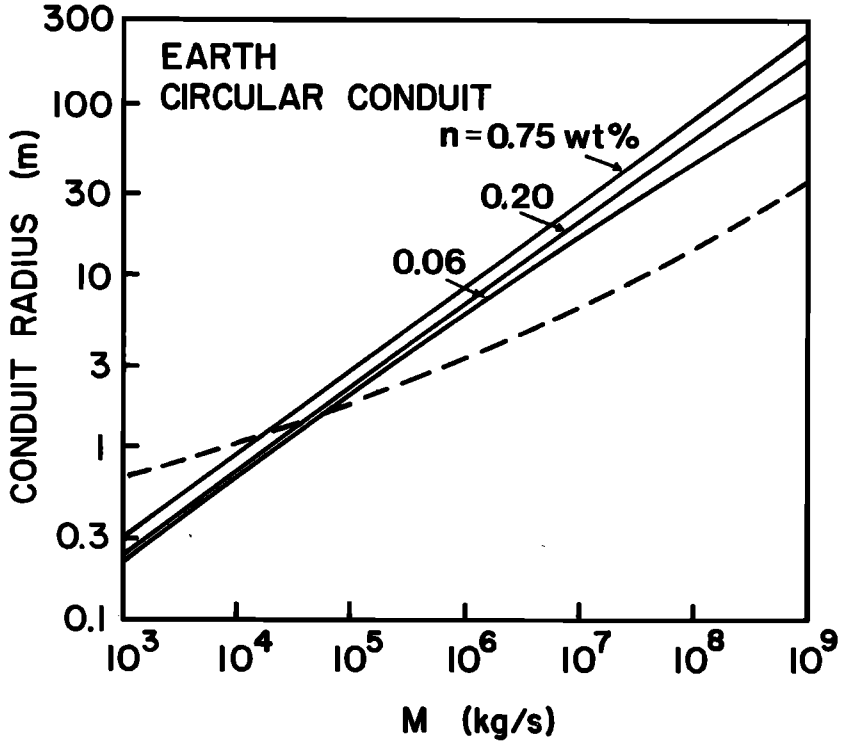

Fig. 6*a*

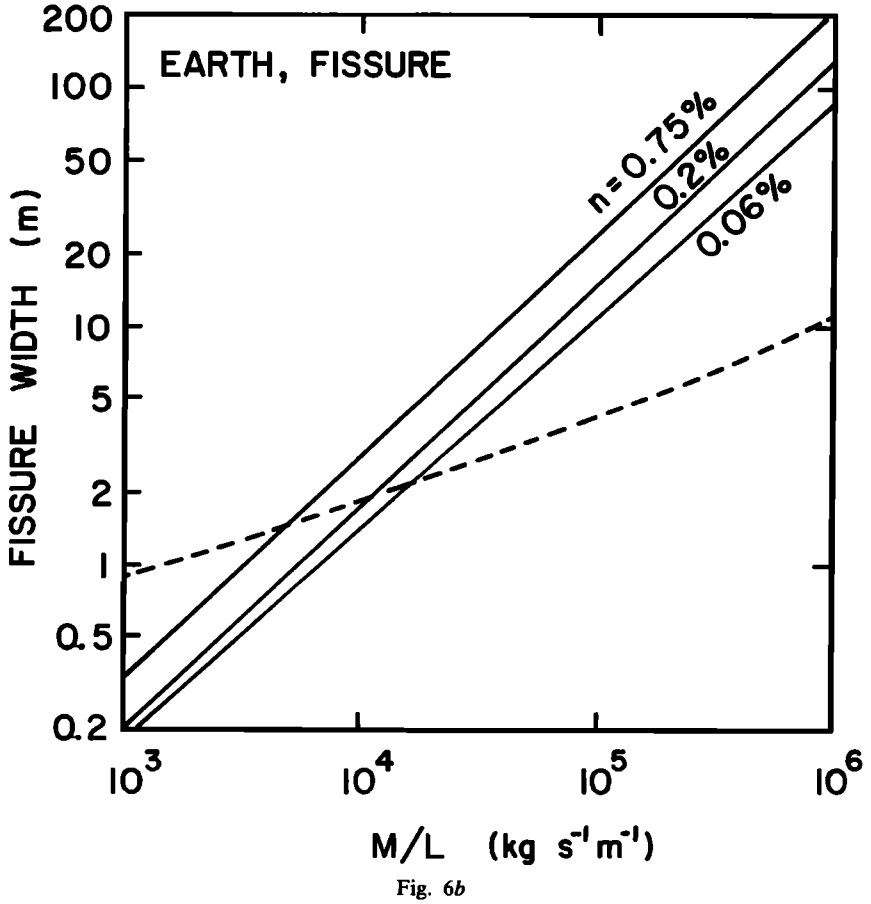

Fig. 6*b*

Fig. 6. Variation of surface vent radius with mass eruption rate, M, for a circular vent (Figure 6*a*) and of surface vent width with mass eruption rate per unit length of fissure M/L for an elongate vent (Figure 6*b*) for exsolved magma water contents of 0.75, 0.2, and 0.06 wt %. The dashed curve shows the corresponding radius or width below the depth where water begins to exsolve in each case.

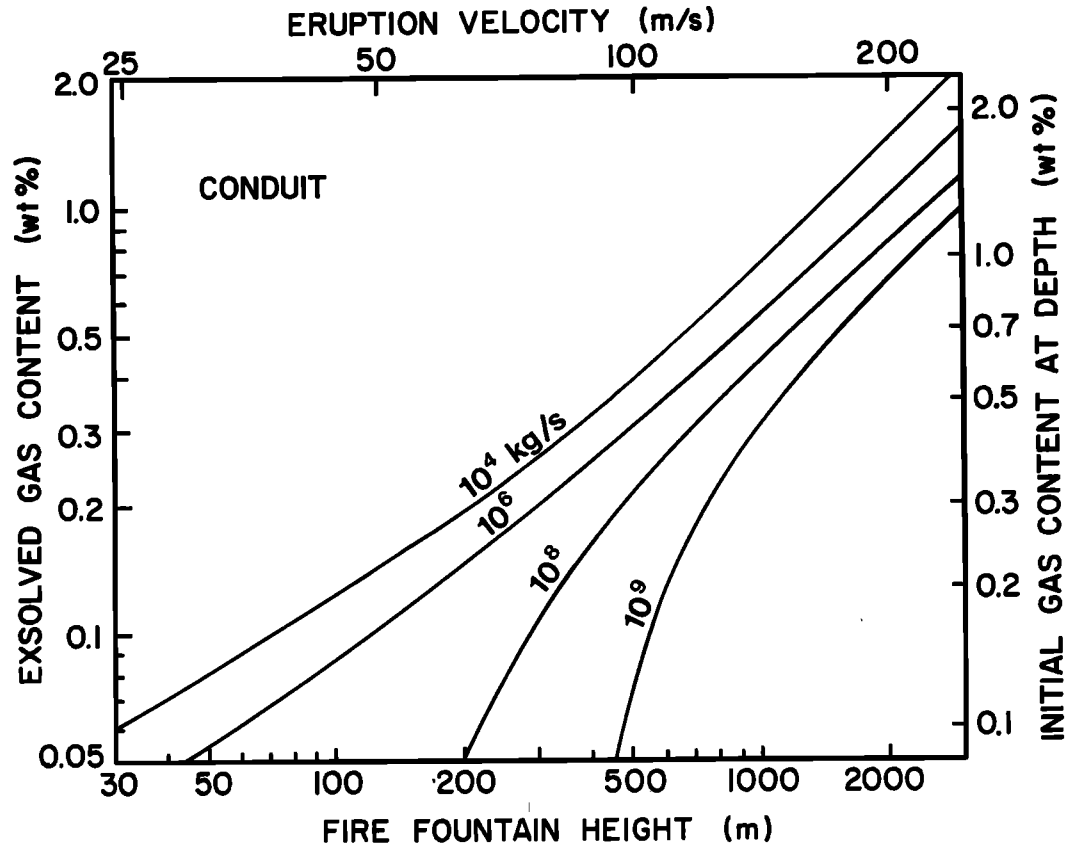

Fig. 7*a*

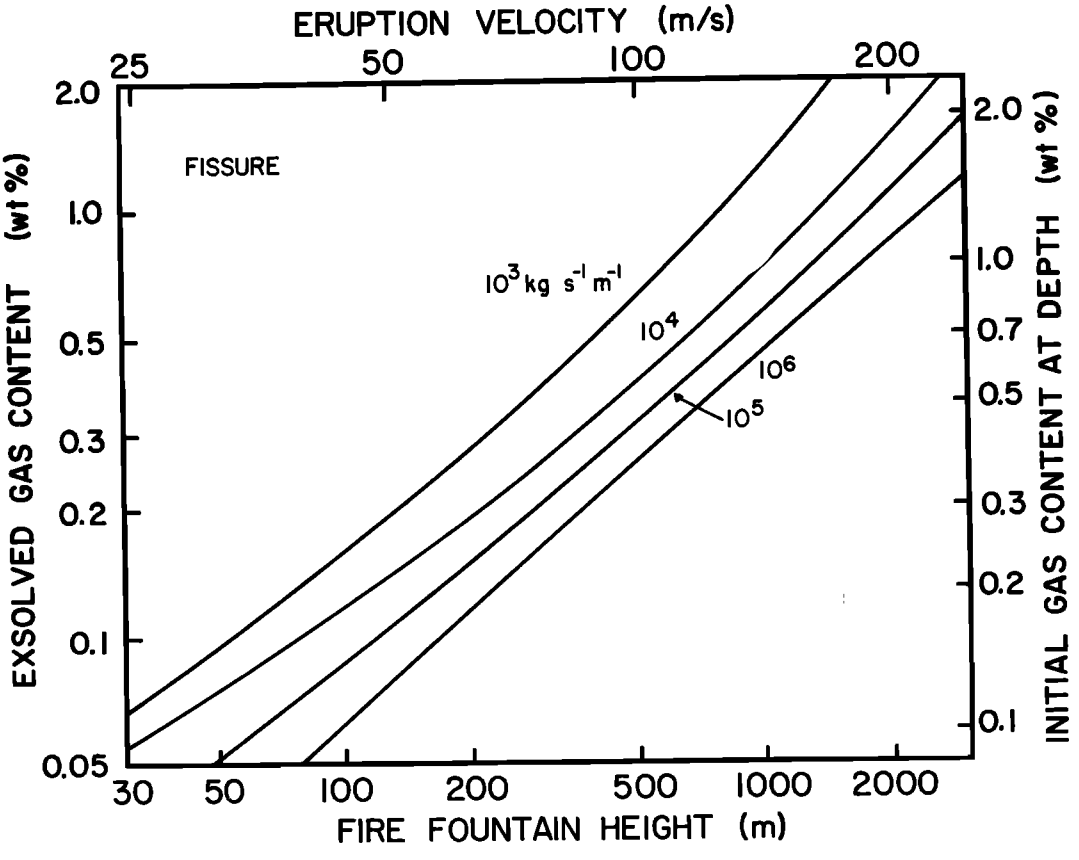

Fig. 7*b*

Fig. 7. Summary of results of calculations for terrestrial eruptions of basalts with density 2800 kg/m^3 and viscosity 300 Pa s through circular conduits (Figure 7*a*) or elongate fissures (Figure 7*b*). The abscissa shows vertical eruption velocity in the vent (at the top) and corresponding maximum fire fountain height (at the bottom) as a function of exsolved water content (on the left) and corresponding total water content (on the right) for a series of effusion rates labeled in kg/s for circular vents (Figure 7*a*) or kg s^{-1} m^{-1} for fissures (Figure 7*b*).

TABLE 7. Values of the Factor K to be Used in Correcting Released Gas Contents Obtained From Figure 7*a*

	M, kg/s			
n_{app}, wt %	10^4	10^6	10^8	10^9
1.0	1.00	1.01	1.01	1.02
0.3	1.00	1.05	1.11	1.15
0.1	1.03	1.07	1.17	1.26

is not important. Figure 7*b* then leads to exsolved gas contents in the range 0.11 to 0.18 wt %. During the 1961 Askja basaltic eruption, fire fountains reached 300 to 500 m, while the output rate was close to 0.9×10^4 kg s^{-1} m^{-1} [*Thorarinsson and Sigvaldason,* 1962]. Again, the exact value of viscosity is not critical; the implied gas contents range from 0.26 to 0.40 wt %. Although representing only a very small sample, these two eruptions are probably typical of Icelandic basaltic activity. The range of released gas contents deduced, 0.11 to 0.40 wt %, corresponds to a range of initial gas contents from 0.18 to 0.57 wt %. This range is very similar to that found by *Moore and Schilling* [1973] by analysis of largely undegassed basalts dredged from the Reykjanes Ridge off Iceland: all but two samples lay in the range 0.18 to 0.43 wt %, and there was a general trend of increasing gas content with proximity to Iceland.

During the 1959–1960 eruption of Kilauea Iki crater, Hawaii [*Richter et al.,* 1970], most of the fire-fountaining activity was from a single (conduit-type) source. Values were recorded for the maximum output rate of magma (3 to 12×10^5 kg/s) and the fire fountain height (300 to 580 m) during several phases of the eruption (phases were numbered from 1 to 17). Figure 7*a* and Table 7 show that, once again, knowledge of the magma viscosity is not essential; some values of observed output rate and fountain height and deduced exsolved gas content are for phase 1, 3.3×10^5 kg/s, 370 m, 0.24 wt %; for phase 7, 6.5×10^5 kg/s, 430 m, 0.25 wt %; for phase 12, 1.2×10^6 kg/s, 300 m, 0.19 wt %; and for phase 16, 1×10^6 kg/s, 440 m, 0.27 wt %. The gas contents all lie in the range 0.19 to 0.27 wt %.

D. *Pyroclast Sizes, Bubble Coalescence and Strombolian Activity*

1. Bubble and pyroclast sizes. We have shown (section IV*A*) that magmatic gas bubbles are able to grow until they are close-packed in all terrestrial magmas with more than about 0.06 wt % water. Magma fragmentation is anticipated when such close packing occurs [*Sparks,* 1978]. The sizes of the largest gas bubbles present at the level where close packing occurs are important in that they exert a strong control on the sizes of the pyroclastic clots and droplets produced by the breaking of the thin liquid films separating adjacent bubbles.

The size of a liquid body isolated by the collapse of the walls of several bubbles will be comparable to the size of the largest bubbles involved. The isolated clot or droplet may itself contain other, smaller bubbles. As magma disruption proceeds and the mean gas pressure decreases as the erupting fluid moves upward, the trapped bubbles will themselves expand. They may break through to the surface of the clot individually and release their gas (in which case, surface tension forces may ultimately shrink the clot by a volume equal to the volume of the bubble at the moment of bursting). Alternatively, several such trapped bubbles may interact to produce a second generation of disruption of the original clot into a number of smaller clots. These, in turn, may contain even smaller trapped bubbles.

This disruption process will proceed either until the gas pressure has reached that of the atmosphere or until the liquid has acquired a high enough yield strength (as a result of cooling or the rheological changes resulting from the degassing [*Sparks and Pinkerton,* 1978]) to support the residual gas pressures in the bubbles. The size of the largest gas bubble expected to remain trapped by the time that the external pressure reaches that of the atmosphere will be greater than the size of the largest bubble present at the fragmentation level by a factor equal to the cube root of the ratio of the pressures at the fragmentation depth and the surface (as long as the magma yield strength is negligible and the gas expansion is nearly isothermal).

We have used the computer program described by *Sparks*

TABLE 8. Values of the Factor K to be Used in Correcting Released Gas Contents Obtained From Figure 7*b*

	M/L, kg s^{-1} m^{-1}			
n_{app}, wt %	10^3	10^4	10^5	10^6
1.0	1.00	1.00	1.01	1.02
0.3	1.01	1.02	1.03	1.05
0.1	1.02	1.07	1.10	1.15

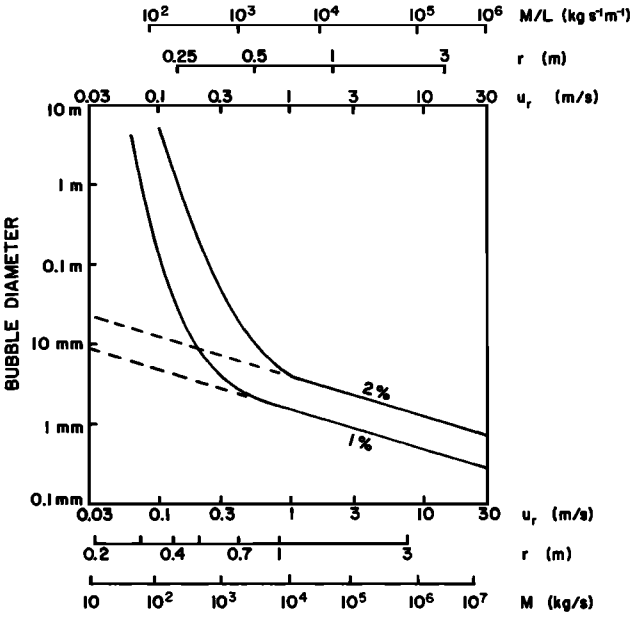

Fig. 8. Variation of maximum H_2O bubble diameter with magma rise velocity u_r for a terrestrial basalt with density 2800 kg/m^3 and viscosity 300 Pa s. The scales at the top give the mass eruption rate per unit length of fissure M/L and the fissure half width r at depths great enough that no water has exsolved corresponding to the rise velocities if the eruption occurs through an elongate fissure; the scales at the bottom give the mass eruption rate M and conduit radius r for a circular conduit. The curves are labeled with the total magma water content in wt %. At rise speeds greater than about 1 m/s, bubble coalescence is negligible, and the diameters given are those at the appropriate magma fragmentation depth; the effects of neglecting bubble coalescence at lower rise speeds are shown by the dashed lines. At the lowest rise speeds the diameter given is the equivalent volume sphere diameter of the largest bubble at a depth equal to its radius. Such bubbles in reality have a spherical cap shape [*Sparks,* 1978] and have maximum horizontal diameters about 1.6 times larger than the values shown.

[1978] to compute the maximum sizes of isolated bubbles at the fragmentation depth as a function of water content, magma rise speed, and viscosity; our numerical solutions for the magma rise model automatically give the pressure at the fragmentation depth, and so the largest bubble sizes at atmospheric pressure can also be found. Figure 8 shows some results for total water contents of 1 and 2 wt % for a basalt with $\eta = 300$ Pa s. The numerous horizontal scales show the mass flow rate and conduit radius below the fragmentation level corresponding to the various rise velocities for circular conduits and also the mass flow rate per unit length and half width corresponding to the same velocities for fissures. The dashed lines and their extensions give maximum bubble diameters at the fragmentation level. The diameters implied for water contents up to 1 wt % and for effusion rates similar to those found in section IV*C3* are of order a few millimeters and match closely the sizes of most vesicles found in basaltic ejecta [*Sparks*, 1978] and also the sizes of the larger nonvesicular basaltic lapilli [*Macdonald*, 1972].

2. Bubble coalescence. A major complication to the idealized picture of the steady rise of a magma carrying embedded gas bubbles occurs when the rise speed of the bubbles through the magma becomes an appreciable fraction of the rise speed of the magma in the crust. Large bubbles will overtake and, under favorable circumstances, coalesce with smaller ones. The resulting increase in volume will lead to an increase in rise speed and an increased opportunity to overtake more small bubbles: clearly, a runaway situation may eventually develop in which very large bubbles arrive intermittently at the surface of the magma, having swept up many smaller bubbles. We take this circumstance to be the origin of the strombolian eruption style.

We have built the process of bubble coalescence into *Sparks'* [1978] bubble rise computer program as follows. Let $N(R)$ be the number of bubbles in the radius range R to $R + dR$ associated with a volume V_1 of the magmatic liquid. We assume that at any level below the surface the total size distribution of bubbles is such that an equal mass of gas resided in each size interval. This is a crude attempt to take account of the fact that new, small bubbles are constantly nucleating with diameters of about 10 μm [*Sparks*, 1978], while there is always a sharp cut-off at a finite, large bubble size representing the current size of the bubble which first nucleated; thus there are many more small bubbles than large ones, and we can put

$$N(R) = A'/R^3 \tag{34}$$

where A' is a constant to be determined. The mass q of a bubble of radius R is $\frac{4}{3}\pi R^3 \rho_g$, where ρ_g is given by (9), so that the total gas mass T_g is

$$T_g = \int_{R_S}^{R_L} N(R)dq = \int_{R_S}^{R_L} N(R)4\pi R^2 \rho_g \, dR = 4\pi\rho_g A' \cdot \int_{R_S}^{R_L} \frac{dR}{R} = 4\pi\rho_g A \ln (R_L/R_S) \tag{35}$$

where R_L is the radius of the locally largest bubble and R_S is the radius of the smallest bubble present, always taken to be 5×10^{-6} m [*Sparks*, 1978]. However, the total gas mass is related to the total liquid mass via n, the exsolved gas fraction,

$$T_g = nV_1\rho_1 \tag{36}$$

Equating the two expressions for T_g and substituting from (9) for ρ_g give

$$A' = \frac{nV_1\rho_1 QT}{4\pi mP \ln (R_L/R_S)} \tag{37}$$

Thus the total volume occupied by the gas bubbles is V_b, where

$$V_b = \int_{R_S}^{R_L} N(R)4\pi R^2 \, dr = \frac{nV_1\rho_1 QT}{mP} \tag{38}$$

and the local fractional volume of bubbles is F_b, where

$$F_b = \frac{V_b}{(V_b + V_1)} = \frac{n\rho_1 QT}{n\rho_1 QT + mP} \tag{39}$$

Consider the bubbles in the radius range R to $R + dR$: they rise through the liquid with a speed $W(R, t)$, where t is the time since nucleation. The calculation of this velocity is already built into *Sparks'* [1978] program. In a time interval dt the largest bubble, rising with a speed W_L, sweeps a volume V_s given by

$$V_s = W_L \pi R_L^2 \, dt \tag{40}$$

and overtakes a fraction $F_0(R)$ of smaller bubbles given by

$$F_0(R) = \frac{W_L - W(R, t)}{W_L} \tag{41}$$

It does not absorb all of them, however. Small bubbles follow the liquid streamlines around the large bubble, and it can only be guaranteed that those which initially lie within their own radius of the vertical line of ascent of the large bubble will make geometric contact with it. We assume that all such bubbles are indeed absorbed by the large bubble, and so the fraction both overtaken and trapped is

$$F_t(R) = \frac{R^2}{R_L^2} F_0(R) \tag{42}$$

The total gas volume V_t represented by all these bubbles is found by multiplying the fraction trapped in each size class by the relative volume present in that size class and integrating over the swept volume during the rise time t':

$$V_t = \frac{\pi}{\ln (R_L/R_S)} \frac{(n\rho_1 QT/mP)^2}{(1 + (n\rho_1 QT/mP))} \cdot \int_0^{t'} \int_{R_S}^{R_L} [W_L - W(R, t)]R \, dR \, dt \tag{43}$$

The integral cannot be readily integrated analytically, since $W(R, t)$ is not any simple function of R and t, varying with Reynolds number and other factors [*Sparks*, 1978], and so it is approximated numerically. After each integration step of the bubble rise program the volume V_t is added to that of the largest bubble and the corresponding new bubble size found.

Figure 8 shows, as the solid curves, the effects of bubble interaction for a basaltic magma with viscosity 300 Pa s and total water contents 1 and 2% by weight. At magma rise velocities at depth which are greater than about 1 m/s a steady fire fountain is expected; at sufficiently low rise speeds (less than about 0.1 m/s and so comparable to the lowest speeds allowed for deep magma sources by cooling constraints; see Table 2), discrete strombolian explosions should take place as individual, conduit-filling bubbles reach the surface.

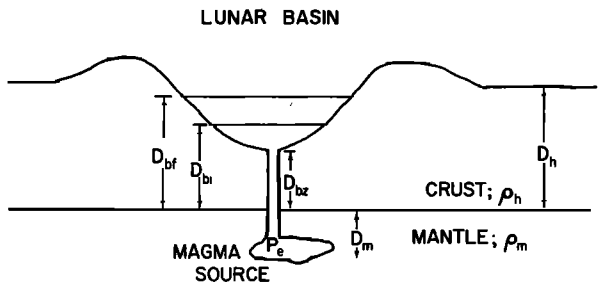

Fig. 9. Sketch of the geometry of eruptions from the upper lunar mantle into mare basins, based on the treatment by *Solomon* [1975].

A much more detailed study of the strombolian process than that given here is needed if detailed interpretations of individual eruptions are to be made, since it is clear that the ejection velocities of explosion products from such eruptions depend critically on the way in which discrete bubbles burst through the magma surface in the vent [*Blackburn et al.*, 1976; *Chouet et al.*, 1974]. For the present we can only conclude that the occurrence of strombolian activity in an effusive eruption implies that the rise velocity of the magma at depth in the conduit system is less than about 0.5 m/s.

V. Ascent and Emplacement of Basaltic Magmas on the Moon

A. Definition of Effective Density Contrast

Solomon [1975] has pointed out that in general, the lunar mare basalts are denser than the crustal rocks through which they must rise to reach the surface and has proposed a mechanism to explain how they can be erupted into the mare basins. Here we extend Solomon's treatment to obtain values for the likely effective density contrasts driving such eruptions. Consider Figure 9 in which a basin of depth $d_b = D_h - D_{bz}$ exists in a crust of density ρ_h and thickness D_h, which overlies a mantle of density ρ_m. A gas-free magmatic liquid of density ρ_l is produced at a depth D_m below the mantle/crust boundary. *Solomon* [1975] argues that a horizontal, constant pressure surface may be defined, passing through the magma source, on which the pressure P_m is dictated by the regional load outside the basin and is given by

$$P_m = \rho_h g D_h + \rho_m g D_m \tag{44}$$

where the variation of g with depth and the finite rock compressibilities are neglected. Hydrostatic balance dictates that the maximum height above the base of the crust to which the basin can be filled is D_{bf} given by

$$\rho_l g(D_{bf} + D_m) = P_m \tag{45}$$

Using (44) for P_m and solving for D_{bf},

$$D_{bf} = \frac{\rho_h D_h + \rho_m D_m - \rho_l D_m}{\rho_l} \tag{46}$$

Thus the basaltic liquid can only be erupted at all if the basin is deeper than $D_{ll} = D_h - D_{bf}$, where

$$D_{ll} = D_h\left(\frac{\rho_l - \rho_h}{\rho_l}\right) - D_m\left(\frac{\rho_m - \rho_l}{\rho_l}\right) \tag{47}$$

If the value of D_{ll} given by this formula is negative, this simply implies that eruptions can take place even without the presence of a basin.

At some general time the magma level will stand at D_{bi} above the base of the crust. The overall pressure gradient driving the eruption, dP/dh, is clearly equal to $P_m/(D_{bi} + D_m)$, so we have

$$\frac{dP}{dh} = \frac{P_m}{D_h + D_m} = \frac{g(\rho_h D_h + \rho_m D_m)}{D_{bi} + D_m} \tag{48}$$

It will be recalled that in the slightly simpler circumstances illustrated in Figure 1 we assumed that the pressure gradient in the erupting magma was equal to the lithostatic gradient. Since in that case we had $P = \rho_h g h$, the gradient dP/dh was just $\rho_h g$. Comparison of this expression with (48) shows that Solomon's mechanism corresponds to replacing ρ_h in all of the equations derived earlier with the quantity ρ_h' given by

$$\rho_h' = \frac{\rho_h D_h + \rho_m D_m}{D_{bi} + D_m} \tag{49}$$

Examination of Figure 9 shows that the lithostatic pressure at the level of the magma source under the basin, P_{lb}, is given by

$$P_{lb} = g[(D_{bi} - D_{bz})\rho_l + D_{bz}\rho_h + D_m\rho_m] \tag{50}$$

which differs from P_m: the difference ΔP is given by

$$\Delta P = P_m - P_{lb} = g[\rho_h d_b - \rho_l(D_{bi} - D_{bz})] \tag{51}$$

At the start of the first basin-filling eruption, when $D_{bi} = D_{bz}$, this differential pressure is a maximum, equal to $g\rho_h d_b$. For a basin depth of $d_b = 5$ km, ΔP would be 227 bars. A stress of this order must be supported somewhere in the lower crust or upper mantle if eruptions into the basin are to be avoided. Furthermore, since the stress to be supported is directly proportional to d_b, a very strong crust would be required to support uncompensated basins many tens of kilometers deep. At the end of all possible eruptions into a basin from a given source depth D_m below the crust, D_{bi} becomes equal to D_{bf} given by (46), and the stress to be supported is a minimum, the value being found on substituting (46) into (51) to be $g[(D_h - D_b)(\rho_l - \rho_h) - D_m(\rho_m - \rho_l)]$. Thus basin-filling eruptions reduce the stress that must be supported at depth below a basin.

Some idea of the trends of numerical values of the variables during basin-filling cycles can be obtained from a simple model with a fixed crustal thickness. According to thermal models of the evolution of the lunar interior [*Solomon*, 1975] we may assume that at about 4 billion years ago the crustal thickness was, say, $D_h = 65$ km. We take reasonable values for the various densities, $\rho_h = 2800$ kg/m^3, $\rho_m = 3400$ kg/m^3, and $\rho_l = 3100$ kg/m^3 and assume that a series of eruptions take place with sources at increasing depths D_m below the crust as the lunar mantle evolves. For the first eruption we take $D_m = 10$ km so that, from (47), the basin depth must be at least $D_{ll} = 5.32$ km: we assume $d_b = 10$ km, so that $D_{bz} = 55$ km. Then the initial crustal stress is $P = 454$ bars. Fractures form in the upper mantle and crust, and an eruptive episode begins. The initial value of ρ_h' is given by (49) with $D_{bi} = D_{bz}$ as 3323 kg/m^3, so that the initial effective density contrast is (3323 − 3100) = 223 kg/m^3. If the magma supply is exhausted when $D_{bi} = 57$ km, so that a thickness of 2 km of basalt has been erupted into the basin, the residual stress in the crust is 353 bars. The value of ρ_h' at the end of the eruption is 3224 kg/m^3, and the effective density contrast has fallen to 124 kg/m^3. If a second eruptive cycle starts at a later time when a new magma

reservoir exists at a depth of $D_m = 30$ km, the new initial value of ρ_h' is 3264 kg/m^3, and the driving density contrast is raised to 164 kg/m^3. If a further 2 km thickness of basalt is erupted before the supply runs out, the stress and density contrast at the end of the eruption are 253 bars and 91 kg/m^3, respectively.

Eruptions would terminate with the basin filled to a depth of 8 km (i.e., to within 2 km of the prebasin surface level) if the final magma supply came from a depth below the crust of $D_m = 44.33$ km. The final driving density contrast would, of course, be zero, and the final stress to be supported at depth would be 52 bars. This pattern of eruptions from steadily increasing depths can maintain the driving density contrast at a value in the range 100 to 250 kg/m^3, while steadily reducing the crustal stresses. It was for this reason that a density contrast of 200 kg/m^3 (together with a source depth of order 100 km) was used in calculations in section III*A*.

B. Volatiles: Composition and Solubility

There is still some dispute as to the composition of possible volatiles in lunar magmas. Calculations and measurements on returned lunar mare basalts by *Sato* [1976, 1977] imply that an important source of volatiles in these magmas was a chemical reaction at pressures less than about 170 bars between carbon and iron oxides to produce metallic iron, CO, and CO_2. Thermodynamic arguments suggest that CO becomes dominant as the pressure decreases. From the measured amounts of nonmeteoritic iron in lunar basalts, *Housley* [1978] deduced that 250 to 750 ppm CO was typically produced in the mare basalts as they erupted. Since there is no strong evidence to the contrary, we assume that CO was the major volatile driving lunar eruptions.

There is no information on the kinetics of the reactions at the molecular level between carbon grains and iron oxides, and so we cannot calculate the CO production rate during the rise of a lunar magma. However, trial calculations have shown that the final eruption conditions of the magma are sensitive only to the total amount of CO produced, not to the detailed variation of production rate with depth. Accordingly, we make the convenient assumption that the amount of CO produced, n_p, increases linearly to the surface from the depth where production starts at a pressure of 170 bars (about 3.5 km). Then, if n_f is the final amount of exsolved CO selected for any particular model calculation, n_p is given by

$$n_p = n_f\left(1 - \frac{h}{h_z}\right) \qquad h < h_z \tag{52}$$

with $h_z = 3.5$ km. The gas produced is only exsolved if n_p is greater than n_d, the solubility at any depth. Thus n is defined as $(n_p - n_d)$ when the value is positive and zero otherwise. There are no data available on the solubility of CO in silicates: we are forced to assume, for the purposes of modeling eruptions, that the solubility of CO is the same as that of CO_2 given by (31).

Figure 2 includes examples of the variation of $(n_p - n_d)$ with depth. Because of the effectively zero atmospheric pressure on the moon, there must be some form of disruption in an erupting lunar magma unless that magma is completely gas-free (or has a sufficiently large yield strength to retain gas bubbles at a finite pressure). Magma disruption may be expected to occur at a depth of about 41 m for a final CO content of about 750 ppm and at a depth of 14 m for 250 ppm.

C. Lack of Atmosphere: Effect on Steadily Erupting Fluids

In the case of a lunar eruption some care is needed in treating the gas pressure near the surface. On a planet with an atmosphere the total pressure at any depth is composed of two contributions, one from the weight of the overlying rocks and the other from the weight of the atmosphere. As a magma rises through a vent, the rock contribution becomes zero, and the pressure becomes that of the atmosphere. On earth the gravity is such that the overlying rock alone exerts a pressure of 1 bar at a depth of about 3 m. Thus the presence of the earth's atmosphere ensures that the fractional change in pressure is very small over the last few meters beneath the surface. In the lunar case the fractional pressure change in the expanding magmatic gas becomes very large over the last few meters if it is assumed that the external pressure is zero. The vertical velocity of the disrupted magma increases rapidly toward the surface, but even so a large increase in cross-sectional area is needed to accommodate the motion if the pressure is to remain lithostatic within the regolith. Since the gas phase must expand sideways to occupy the whole of the vent, significant horizontal velocity components occur, and the energy equation must be modified to take account of this fact: the form given in (1) applies only to one-dimensional motion.

A complete solution to this problem would involve detailed treatment of the three-dimensional flow field in the vent. Fortunately, however, this is not necessary for the present purpose. As long as the horizontal velocity component is considerably less than the vertical component, a locally conical approximation to the flow field may be used. Evaluation of the average horizontal velocity in terms of the horizontal velocity at the edge of the conduit or fissure shows that if u is still identified as the upward velocity in the center of the vent, the total kinetic energy term, equal to $\frac{1}{2}u^2$ in the one-dimensional case, may be approximated by $\frac{1}{2}u^2\,[1 + Y(dr/dh)^2]$, where $Y = 1/3$ (for a fissure) and 1/5 (for a circular conduit). For convenience, the same formula is used when dr/dh, the rate of vent widening toward the surface, becomes large; however, the term $Y(dr/dh)^2$ is not allowed to increase to values greater than unity: this corresponds to the limiting case where energy is shared equally by the horizontal and vertical velocity components. The complex motions approximated by the above treatment only set in near the surface, roughly at the level where the radius of the conduit or fissure is equal to the depth.

D. Steady Lunar Eruptions

The considerations presented earlier for terrestrial eruptions, relating to the opening of vents and the early stages of eruptions, apply in the same way to lunar events and need no further discussion. As before, we make the simplifying assumption that the pressure in the erupting material is everywhere lithostatic once fairly steady eruption conditions are reached. Figures 10 and 11 show some examples of the variation with depth of fissure or conduit width and upward velocity for a number of effusion rates of a lunar basalt with viscosity 10 Pa s and released gas content 750 ppm CO. The patterns are generally similar to those for terrestrial eruptions except for the more rapid increase of both vent width and eruption velocity within the last few meters of the surface as the effects of the negligible external pressure dominate. The relative increase in both of these quantities is less for eruptions with lower gas contents.

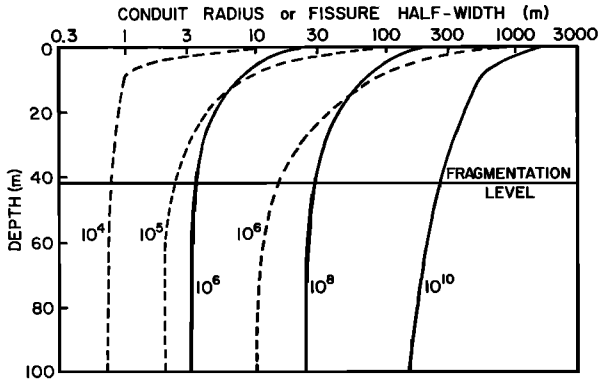

Fig. 10. Variation with depth below the surface of the conduit radius (solid curves) or fissure half width (dashed curves) for lunar eruptions of a basalt with density 3000 kg/m^3, viscosity 10 Pa s, and final exsolved CO content 750 ppm. The solid curves are labeled by mass eruption rate in kg/s and the dashed curves by mass eruption rate per unit fissure length in kg s^{-1} m^{-1}.

1. Lunar vent sizes. Because of the very rapid outward flaring expected within the regolith zone it is not a simple matter to specify the sizes of surface vents. The present thickness of the regolith in most lunar highland is up to about 15 m [*Cooper et al.*, 1974], whereas at the time of the major volcanic episodes (3 to 4 billion years ago) the regolith thickness may have been less by a factor of about 2. Continuing regolith development may have redistributed surface materials to the extent that vent shapes within a few meters of the surface have been radically changed. Only in cases where some form of pyroclastic cone formed around the vent with a height substantially greater than the present regolith thickness is it probable that some vestige of the original structure would be recognizable now. This is particularly true for effusive eruptions where the vent may be left almost completely blocked by the last magma to emerge.

As an extreme alternative, if the local magma source is at shallow depth, the evacuation of the magma reservoir may be compensated by subsidence of the surface rocks near the vent leading to the production of a caldera comparable in horizontal extent to the size of the initial magma body. In view of the petrological evidence that lunar basalts appear to have reached the surface directly from depths of the order of 100 km or more [*Kesson and Lindsley*, 1976; *Papike et al.*, 1976] it is doubtful if this second alternative is common. In either case, however, it will be hard to associate the size and shape of the apparent surface features with the original vent geometry. The only safe generalization is that the fractional increase of the length of an elongate fissure source will be less than the fractional change in its width.

For those cases where only regolith development has modified the initial vent shape it is proposed that the vent size at a depth equal to the present regolith thickness may be comparable to the apparent size of presently observable depression features. Accordingly, Figures 12*a* and 12*b* give the relevant parameter (radius for a conduit, half width for a fissure) as a function of released gas content and effusion rate.

We note that for eruptions from fissures, even effusion rates 10 times larger than those estimated for the Columbia River basalt flows on earth (about 3×10^4 kg s^{-1} m^{-1} [*Swanson et al.*, 1975]) would only require vents less than 10 m wide. These would be hard to locate in most orbital photographs unless accompanied by other features such as constructional pyroclastic deposits or collapse depressions.

2. Magma fragmentation. At the fragmentation level a lunar magma disrupts into a spray of droplets and clots whose sizes will be controlled at least partly by the sizes of the largest bubbles present in the way discussed earlier for the terrestrial case. However, the fact that the released gas must expand to essentially zero final pressure means that even the smallest bubbles will attempt to expand to an infinite size. Although gas release may tend to produce undercooling of the melt by raising the solidus and liquidus temperatures [*Sparks and Pinkerton*, 1978], this may be compensated by the fact that gas exsolution is an exothermic process [*Burnham and Davis*, 1974]; also, some lunar basalts may have been superheated on eruption [*Ringwood and Kesson*, 1976], and much more thorough disruption of the magma droplets is to be expected in a lunar basaltic eruption than in any terrestrial eruption. A wide range of nonvesicular droplet sizes, from diameters comparable to the sizes of the largest bubbles present at fragmentation down to diameters comparable to the sizes of the smallest bubbles capable of nucleating, about 10 μm, is expected.

In an attempt to calculate the sizes of the largest noncoalescing bubbles present in lunar basalts we have modified the computer program developed by *Sparks* [1978] to solve the growth of H_2O bubbles in terrestrial magmas to deal with the lunar case. As with the case of gas solubility, the material properties of CO_2 were substituted for those of CO where the latter were not known. Figure 13 shows the variation of the largest bubble diameter at the level of magma fragmentation as a function of final released gas content and M (for a conduit) or M/L (for a fissure) for a lunar basalt with viscosity 10 Pa s. Maximum bubble sizes range from a few millimeters at the lowest effusion rates which can occur to a few hundred microns at the highest expected. The possibility of bubble coalescence has been included in the lunar calculations, and the results are shown in Figure 13. At rise velocities greater than about 3 m/s, coalescence is negligible, while at rise velocities less than 0.3 m/s, bubbles up to several centimeters in diameter may be present at the fragmentation level.

To summarize, in nonstrombolian eruptions, lunar pyroclasts should be relatively free of gas inclusions and be present in the total size range from a few millimeters to a few tens of microns. Where strombolian activity occurs, the droplet size range will extend to somewhat coarser droplets. These sizes

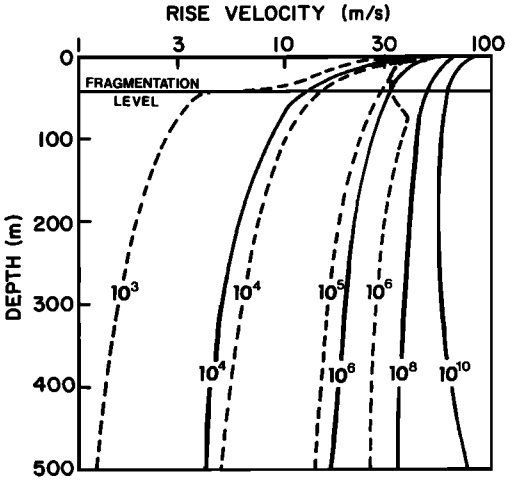

Fig. 11. Variation with depth below the surface of the upward rise velocity of magma (or magma disruption products above the fragmentation level) in lunar eruptions. Curves and labels are as for Figure 10.

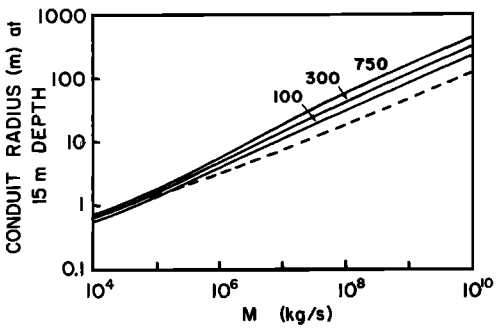

Fig. 12*a*

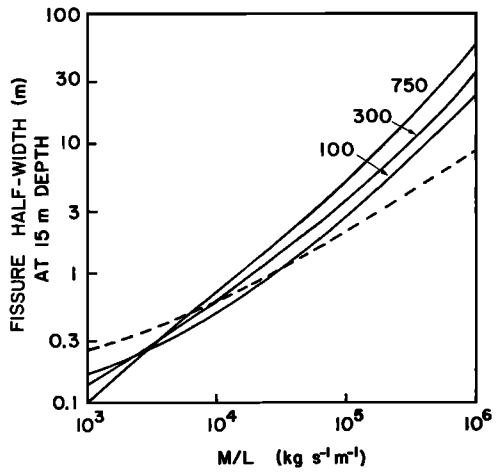

Fig. 12*b*

Fig. 12. Circular conduit radii (Figure 12*a*) and elongate fissure half widths (Figure 12*b*) at a depth of 15 m below the present lunar surface for basaltic eruptions with exsolved CO contents of 750, 300, and 100 ppm, given as a funtion of mass eruption rate M (Figure 12*a*) or mass eruption rate per unit fissure length M/L (Figure 12*b*). The radius or half width below the depth where CO release begins is shown by the dashed line.

are very similar to those of the various types of glass spheres found in the Apollo regolith samples and already widely accepted as being of pyroclastic origin [*Heiken and McKay*, 1977].

3. Ejection velocities and ranges of coarse pyroclasts in steady eruptions. Shortly above the magma fragmentation level, the released droplets move as discrete individuals in the stream of released gas. All particles whose terminal velocities in the gas are small relative to the upward velocity of the gas in the vent stay locked to the gas motion. They and the gas together form a compound fluid to which the equations we have presented earlier apply just as well as to a continuous magmatic liquid containing bubbles. However, if droplets are sufficiently large, their motion relative to the gas cannot be ignored; they lag behind the gas motion and accumulate progressively in the vent. If we assume, for the moment, that not too many of the droplets are large, so that our calculated velocities are adequate, then we can compute (using the method of *Walker et al.* [1971]) the size of the droplet which will have a terminal velocity in the gas equal to the gas rise speed at any level between the fragmentation depth and the surface. This droplet size marks the boundary between droplets which stay locked to the gas and those which decouple from it. Table 9 shows the results of these calculations for a point just above the fragmentation level for released gas contents in the range 100 to 750 ppm and all effusion rates of interest. In all cases the calculated droplet size would decrease if the calculation were performed for a shallower depth. This fact emphasizes the point that in lunar eruptions the released gas eventually escapes completely from the eruption site (whereas on earth it is always incorporated into an eruption cloud of some sort), and all pyroclasts, however small, must decouple from the radially expanding gas cloud eventually; we shall return to this point shortly. However, for the moment we can say with certainty that droplets or clots bigger than the sizes given in Table 9 will decouple at once from the gas flow and proceed up the vent with an initial speed equal to the magma rise speed just below the fragmentation level.

If the limiting sizes in Table 9 are compared with the expected largest bubble, and hence droplet, sizes in Figures 13, it is clear that at high effusion rates all the droplets will stay coupled to the gas flow, and thus that velocity/depth curves such as those shown in Figure 11 will be accurate. However, at low effusion rates a significant fraction of the droplets will decouple from the general gas flow and pursue quasi-ballistic trajectories. We can define a limiting effusion rate, M_A for conduits or $(M/L)_A$ for fissures, as a function of released gas content, above which a negligible number of droplets will decouple from the gas flow in the vent. This limiting effusion rate is plotted as a function of n in Figures 14*a* and 14*b*.

For those cases where droplets do decouple from the gas flow at once, our numerical models provide both the rise speed and the slope of the vent wall at the fragmentation level, and we can compute the trajectories out of the vent and find the maximum range across the surface of the larger droplets. If u_z is the mean upward velocity of the magma, r_z the conduit radius or fissure half width, and $(dr/dh)_z$ the slope of the vent wall at the fragmentation level at depth h_z, then the range is X given by

$$X = r_z + \frac{u_z}{g}\left(\frac{dr}{dh}\right)_z [u_z + (u_z^2 - 2gh_z)^{1/2}] \qquad (53)$$

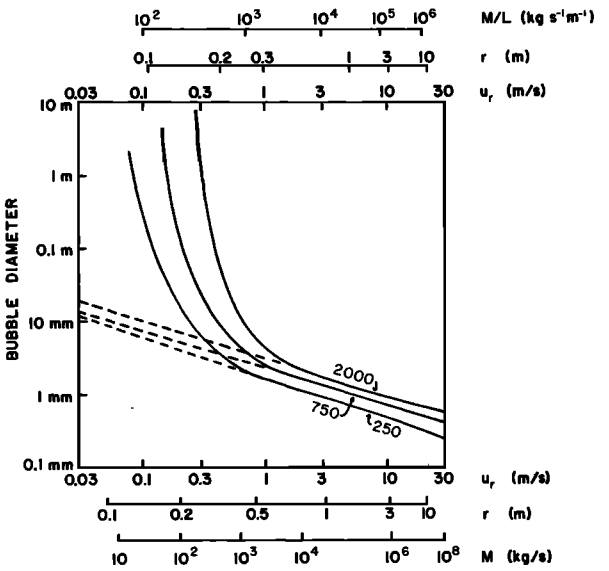

Fig. 13. Variation of maximum CO bubble diameter with magma rise velocity u_r for a lunar basalt with density 3000 kg/m^3 and viscosity 10 Pa s for exsolved Co contents of 2000, 750, and 250 ppm. All other details correspond to those given in the caption to Figure 8.

TABLE 9. Values of the Diameter in Millimeters of Dense Liquid Droplets Having Terminal Velocities in the Gas Stream Equal to the Gas Velocity Just Above the Fragmentation Level for Lunar Magmas With Viscosity 10 Pa s

	M,* kg/s				
n, ppm	10^2	10^4	10^6	10^8	10^{10}
750	2	22	150	240	500
300	0.3	7	37	69	180
100	0.1	1.6	6.7	12	60
	M/L,† kg s^{-1} m^{-1}				
n, ppm	10^2	10^3	10^4	10^5	10^6
750	0.1	2.6	32	120	320
300	0.05	1.0	10	30	40
100	0.01	0.3	2.0	5.6	6.7

Here n is the released weight fraction of CO, M is the mass eruption rate in a circular conduit, and M/L is the mass eruption rate per unit length in a fissure.

* Conduit.

† Fissure.

Clearly, droplets will not leave the vent at all unless the velocity u_z is greater than $(2gh_z)^{1/2}$. We can define a second limiting effusion rate, M_B for conduits and $(M/L)_B$ for fissures, below which no decoupling droplets can leave the vent; this second limiting effusion rate is also shown in Figures 14*a* and 14*b*. Consider the case of a conduit. For all gas contents at which M_A is greater than M_B there are only two possible scenarios. If the actual effusion rate in a given eruption M is greater than M_B, all droplets leave the vent; if M is less than M_B, a finite number of large droplets do decouple from the gas flow and cannot leave the vent. They are eventually deposited on the vent walls. If, however, M_A is less than M_B, as is true for gas contents less than about 300 ppm, then there are three scenarios. If M is less than M_A, a finite number of coarse droplets are deposited inside the vent. If M is greater than M_A but less than M_B, some coarse droplets do decouple from the gas flow but leave the vent to form a local pyroclastic deposit. If M is greater than M_B, no droplets decouple from the gas flow within the vent.

Exactly equivalent arguments apply for fissure eruptions, and these combinations of circumstances are summarized in Figures 14*a* and 14*b*. If (53) is used to evaluate the ranges of coarse droplets forming a localized deposit outside the vent, it is found that the maximum possible ranges are about 20 m in the case of conduit eruptions and about 30 m for fissure eruptions. Thus, if our assumption that fluid lunar basalts undergo almost complete fragmentation is correct, it is clear that only very localized pyroclastic structures will be formed from the coarser ejecta.

For the sake of completeness we consider the possibility that the above assumption is incorrect, and that even with high gas contents and high effusion rates, steady eruptions produce a large proportion of coarse droplets, i.e., bigger than the diameters given in Table 9. Then (53) enables us to find the maximum range of such ejecta as a function of effusion rate and released gas content. Figure 15 summarizes the results of such calculations and shows that wide, low pyroclastic structures up to tens or hundreds of meters in diameter could be produced.

4. Sorting of small particles in steady eruptions. The findings of the previous section can be elaborated somewhat by considering in more detail the way in which progressively smaller pyroclastic droplets decouple from the steady state eruption cloud over the vent at increasing distances. We have already shown that in a steady lunar eruption a transition must occur in the upper part of the vent from mainly upward motion to radial motion. For a circular conduit/vent system the symmetry dictates that the final motion of the gas and all clasts locked to it is radially outward into a hemisphere. For a fissure source the elongate shape implies that just above the vent the motion will have cylindrical symmetry. At distances much greater than the active fissure length, however, the motion will rapidly tend to hemispherical flow. For simplicity we treat only the purely hemispherical flow case but show retrospectively that most of the results are also applicable to the fissure case.

Since the expanding cloud of gas and clasts is a steady (time independent) system, equations (1), (2), (3), (5), and (8) apply to it with minor modifications; we assume that the gas expansion is largely adiabatic and so use (10) to relate the gas density to the pressure. The main change required is to replace the height coordinate h with a radial coordinate c, measured from the center of the vent at ground level. It is now adequate to neglect both the friction term in (1) and, since the gas volume at the pressures involved is much greater than the total particle volume, the particle volume term in (8). The potential energy term in (1) is modified by noting that the potential energy per unit mass of a hemispherical shell of radius c is $\frac{1}{2}gc$; the required equations become

$$-\frac{dP}{\rho} = u\,du - \tfrac{1}{2}g\,dc \tag{54}$$

$$\frac{d\rho}{\rho} + \frac{du}{u} + 2\frac{dc}{c} = 0 \tag{55}$$

$$\frac{1}{\rho} = \frac{n}{\rho g} \tag{56}$$

with (10) as before.

The main inadequacy of this treatment is that it neglects the effect (on the main part of the cloud of gas and relatively small clasts) of the motion of the relatively large clasts as they decouple from the general flow and fall to the ground. More exact solutions to the problem require complex iterative methods and may be the subject of future study; the present analysis serves to give a general picture of the particle sorting. The above equations are solved by a stepwise numerical integration scheme. The starting conditions for the integration are taken to be the gas contents and velocities just above the fragmentation surface in each of the models treated in the previous section, and the initial value of c is taken to be the conduit radius at this depth. Thus the solutions are referred to distances measured from the fragmentation level rather than the true lunar surface; however, the ranges of droplets of interest are so much greater than the depths of fragmentation surfaces below ground that this is of negligible importance.

The progressive decoupling of clasts is clearly a function of their size distribution. On the basis of earlier arguments the clasts should consist mainly of submillimeters sized droplets; however, we cannot neglect the possibility that a significant number of much larger fragments may be present. We synthesize the fallout of clasts by slowly increasing the value of n, the gas mass fraction in the cloud, with radial distance. A relatively rapid rate of increase of n corresponds to a size distribu-

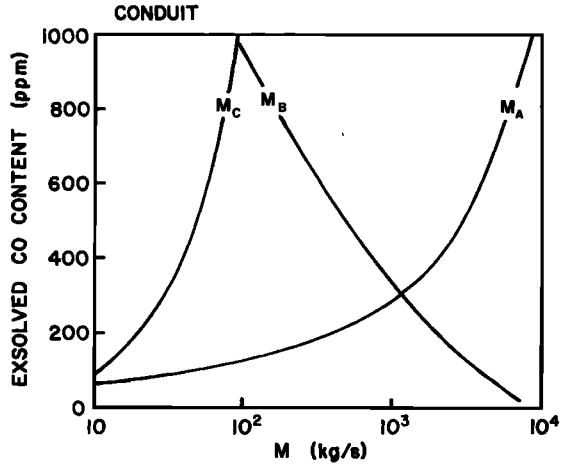

Fig. 14*a*

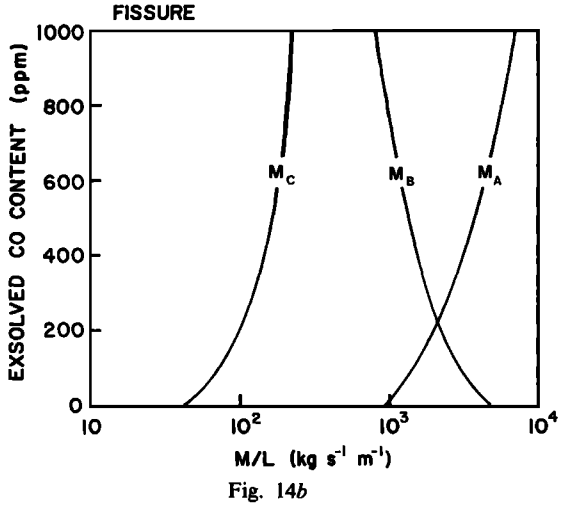

Fig. 14*b*

Fig. 14. Variation with exsolved CO content n of the three limiting effusion rates defined in the text. For circular conduits, Figure 14*a* shows M_A, the mass eruption rate above which a negligible fraction of submillimeter droplets will decouple from the gas flow just above the fragmentation level; M_B, the mass eruption rate below which decoupling droplets cannot be projected over the edge of the vent; and M_C, the mass eruption rate below which strombolian activity will occur. Figure 14*b* shows the corresponding mass eruption rates per unit fissure length for elongate vents.

tion in which coarse particles predominate, while a relatively slow rate of increase represents a predominance of small droplets. Suitable rates of increase to correspond to realistic particle sizes were found by trial and error.

At each stage of the integration a value can be calculated for the diameter of droplet which has a terminal velocity in the gas equal to the local gas speed. Droplets of this size will decouple from the gas flow in the region directly above the vent. At greater horizontal distances it is, of course, only the vertical component of the gas velocity which supports the droplets. Thus a droplet of the above size which happens to be traveling along a nearly horizontal path in the base of the cloud will decouple from the cloud much closer to the vent. The maximum final range reached by a particle of any given size will be obtained if that particle travels along a trajectory which is initially inclined at an angle somewhat greater than 45° to the horizontal. The upward gas velocity component at the radial distance c where it decouples from the flow will then be roughly $1/\sqrt{2}$ (i.e., about 0.7) times the total gas velocity, and so it is the diameter of the particle whose terminal velocity is equal to this latter velocity which will be relevant at any given integration step. Such a particle will progressively lose its vertical support from the gas and will be traveling nearly horizontally at the time it decouples; it will therefore travel a further distance $u^2/2g$, where u is the local total velocity component. Since it separates from the rest of the gas flow at a radial distance c from the vent and has been traveling at an average elevation of about 45°, its horizontal distance is $c/\sqrt{2}$ at this point, and so its total range is D_c, where

$$D_c = \frac{c}{\sqrt{2}} + \frac{u^2}{2g} \tag{57}$$

The above operation is carried out at each integration step for each chosen rate of increase of n with c. It is found in all cases that the calculated released particle size decreases with c rapidly at first and then becomes essentially constant. In each model calculation we record the ratio α by which n has increased and the corresponding total particle range D_c when the limiting size, say d_c, is reached. Gas mass enrichment by a factor α corresponds to a total particle mass decrease by a factor β, where

$$\beta = \frac{1 - n\alpha}{\alpha - n\alpha} \tag{58}$$

Thus each model leads to a prediction that particles much smaller than the diameter d_c can reach a maximum range D_c, provided that they comprise no more than a fraction $(1 - \beta)$ of the total magma mass. A surprising feature of the results is that d_c is not a strong function of magma gas content or effusion rate, always being in the range 4 to 10 mm. Thus the degree of dispersal of the pyroclastic droplets depends critically on whether or not many magma clots larger than a few millimeters in diameter are formed as the magma disrupts. Figure 16 summarizes the results of these calculations, showing the maximum range which submillimeters droplets can reach as a function of the fraction they represent of all the ejecta for several pairs of values of total effusion rate and released magma gas content. Although the results have been calculated for a circular vent source, they are also applicable to fissure sources as long as the length of the active fissure is somewhat smaller than the droplet ranges of interest. Clearly, if submillimeter droplets from only a very small fraction of the total ejecta, they can be expelled to distances of tens of kilometers. If, however, they form the majority of the ejecta, their ranges are much more limited.

For this latter case, which we have argued is likely to be the most common in lunar eruptions, Figures 17*a* and 17*b* show, for circular and fissure vents, the combinations of released gas content n and effusion rate needed to eject droplets to a given maximum range.

5. Deposit accumulation rates and resulting structures in steady eruptions. The types of pyroclastic structure or lava flow formed near a lunar vent will depend on the accumulation rate of ejected magma which will in turn be a function of the mass eruption rate and the exsolved magma gas content. There are two cases to consider.

Gas-free magma: In a completely gas-free magma the magma rise velocity u_f at all depths is given by (12). With no gas expansion to be accommodated there is no particular reason to expect a flared vent shape. A nearly vertical fountain of magma will rise above the vent to a height $u_f^2/2g$; the flow field within it will be upward in the middle and downward

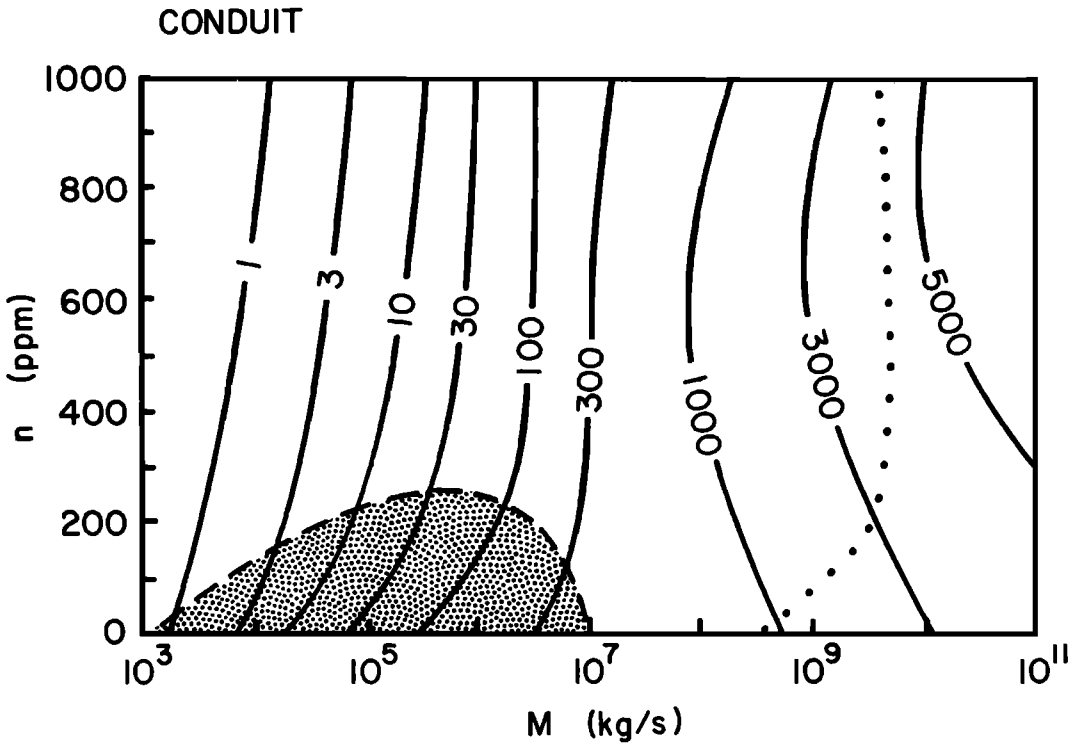

Fig. 15*a*

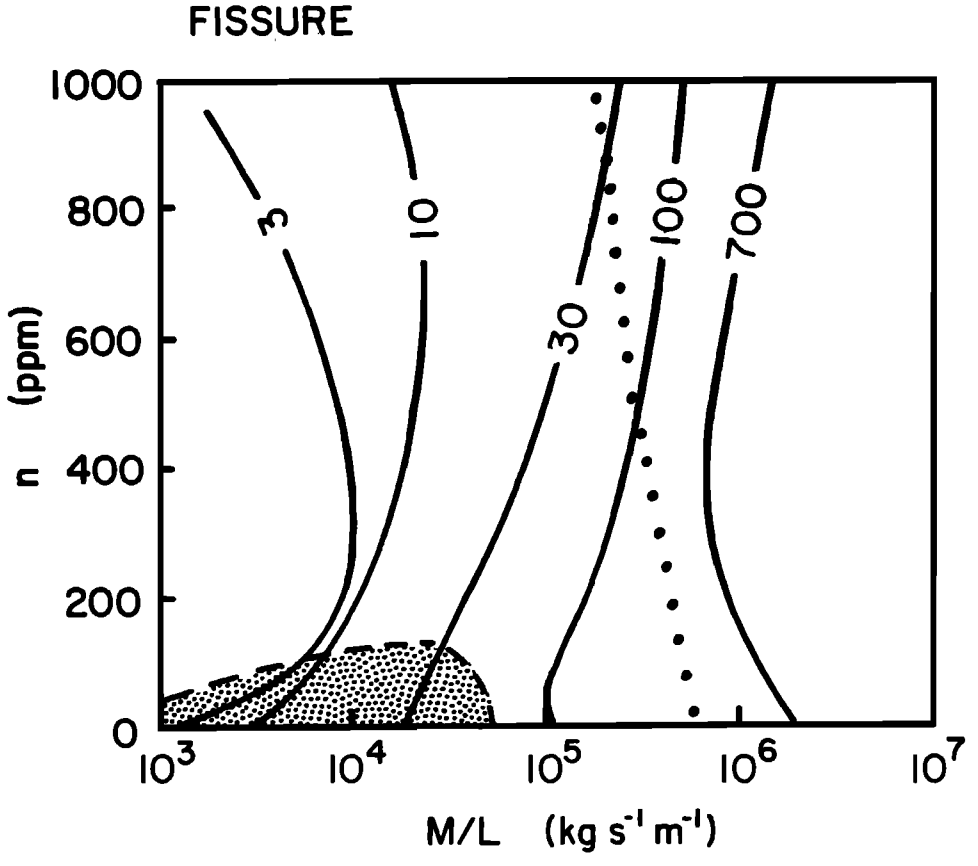

Fig. 15*b*

Fig. 15. Combinations of values of released Co content n and effusion rate required to produce a given maximum ejecta range for lunar eruptions in which the majority of the ejecta are larger than a few millimeters in size. Figure 15*a* is for circular vents and Figure 15*b* for elongate fissures. The solid curves are labeled by the maximum range in meters. The stippled areas show the combinations of circumstances leading to accumulation of cooled pyroclasts if the mean clast size is 0.1 m; all combinations of circumstances to the left of the dotted line lead to cooled deposits if the mean clast size is 1 m.

over the outer surface. Surface wave instabilities may cause magma blobs to separate from the outer surface, but essentially, the magma will arrive back on the ground within one vent radius of the vent edge in a steady stream and coalesce to form a lava flow. This will be true of both conduit and fissure eruptions and will apply for all effusion rates. No pyroclastic structures will be formed. It follows that the presence of a substantial pyroclastic structure around a lunar vent, or the presence of pyroclastics in the nearby regolith, implies that gas was released from the erupted magma.

Steady eruptions with gas present: In all cases where gas is released, there is substantial disruption of a lunar magma and significant dispersal of the eruption products. A number of factors bear on the temperature of the accumulating ejected clots and droplets. If effusion rates are low enough, gas content is high enough, or magma blobs are large enough, the cloud of dispersing objects will be optically thin: radiation from individual clots can escape at once from the cloud. If the clots are big enough or their flight time is short, they may not cool significantly except in a thin surface layer; if they are small enough or the flight time is long, they may cool to complete rigidity. On the other hand, if the eruption cloud is optically thick, the case favored by high effusion rate, low gas content, and small droplets, then only particles in the outer shell of the cloud will cool, and all others will land at magmatic temperatures, irrespective of their size and flight time. An estimate can be made of the optical depth in a cloud of locally uniform density as follows.

Let d be the average particle diameter in the eruption cloud and S be the average interparticle distance. If the particles were arranged in regular layers, the fractional cross-sectional area obscured by the particles in any one layer would be $\phi = \pi d^2/S^2$, and so in a random arrangement the number of such layers required to produce complete obscuration is of order $1/\phi$; at an average spacing S these represent a depth into the cloud of $S^3/\pi d^2$. Statistically, however, some foreground particles obscure background particles rather than obscuring the space between them: the first layer in the cloud obscures a fraction q of the area beyond leaving a fraction $(1 - \phi)$ visible; the second layer leaves a fraction $(1 - \phi)^2$ visible and so on. If we assume J layers are needed to reduce the visible area to a fraction δ, we have

$$(1 - \phi)^J = \delta \qquad J = \ln \phi / \ln(1 - \phi) \tag{59}$$

But ϕ is much less than unity, so $\ln (1 - \phi) \approx -\phi$ and we can put

$$J = -\ln \delta / \phi \tag{60}$$

Thus instead of $1/\phi$ layers we need $(-\ln \delta)$ times $1/\phi$ layers, i.e., more by a factor of $F = (-\ln \delta)$; some values of this factor are for $\delta = 0.1$, $F = 2.3$; for $\delta = 0.01$, $F = 4.6$; for $\delta = 0.001$, $F = 6.9$. Clearly, it will be adequate to take $F \approx 10$. So the cloud will be optically thick if the number of layers, at separation S, is greater than $10/\phi = 10S^2/\pi d^2$, i.e., if the cloud is thicker than $10S^3/\pi d^2$. There is a final complication. We expect in reality a finite range of particle sizes around the average diameter. Let the range be from a factor ϵ less than d to a factor ϵ greater than d. Then if there are, say $(2m + 1)$ classes each containing an equal mass of particles, the average size of the particles in a general class is $d\epsilon^{(k-1-m)/m}$, where k runs from 1 to $(2m + 1)$. The number of particles in a class is proportional to the class size to the power -3, while the cross-sectional area

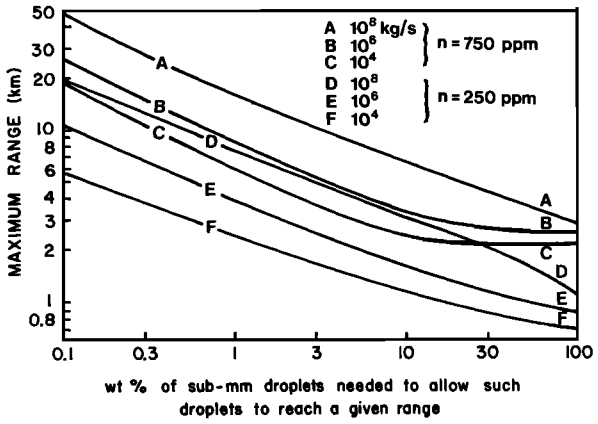

Fig. 16. Maximum ranges of submillimeter ejecta as a function of the mass fraction they represent of all the ejecta for six combinations of mass eruption rate and released CO content in lunar eruptions.

of each particle in the class is proportional to the class size squared, so the total area contributed by any class is proportional to the class size to the power -1. Thus the total cross-sectional area contributed by all the classes is proportional to A_1, where

$$A_1 = \sum_{k=1}^{2m-1} \epsilon^{-((k-1-m)/m)} d^{-1} \tag{61}$$

whereas if all the particles had had the same size, the equivalent total area would have been proportional to A_2, where

$$A_2 = \sum_{k=1}^{2m+1} d^{-1} = (2m + 1)\, d^{-1} \tag{62}$$

It follows that the particles have a total cross-sectional area greater than that found by assuming them all to have the average particle size by a factor G given by

$$G = \frac{A_1}{A_2} = \frac{1}{(2m + 1)} \sum_{k=1}^{2m+1} \epsilon^{(1+(1/m)-(k/m))} \tag{63}$$

Since we really need the value of G corresponding to a continuous distribution of grain sizes, we take the limit of this expression as m goes to infinity which is easy to approximate numerically. Some values are $G = 1.2$, 2, 11, and 72 for $\epsilon = 3$, 10, 100, and 1000, respectively. Since we have argued that the lunar magma droplet sizes should mainly lie in the range 1 mm to 10^{-2} mm, it is appropriate to use $\epsilon = 10$ and so $G \approx 2$. The final estimate of the cloud thickness needed for complete obscuration is thus Λ, where

$$\Lambda = 5S^3/\pi d^2 \tag{64}$$

It does not matter if we make the alternative assumption that particle sizes are much larger than 1 mm as long as the ratio of the sizes of the largest and smallest particles is not too different from the above example.

The average particle spacing in a cloud, S, can be evaluated from the effusion rate, the average particle size d, the particle density (equal to ρ_l), and the maximum range D. For a circular vent producing a mass eruption rate M the number of fragments released per unit time is $N = M/((\pi/6)\, d^3 \rho_l)$. We have shown earlier (section V*D4*) that all particles ultimately follow an approximately parabolic trajectory to their final range (for the whole path if they are large clots which never experience

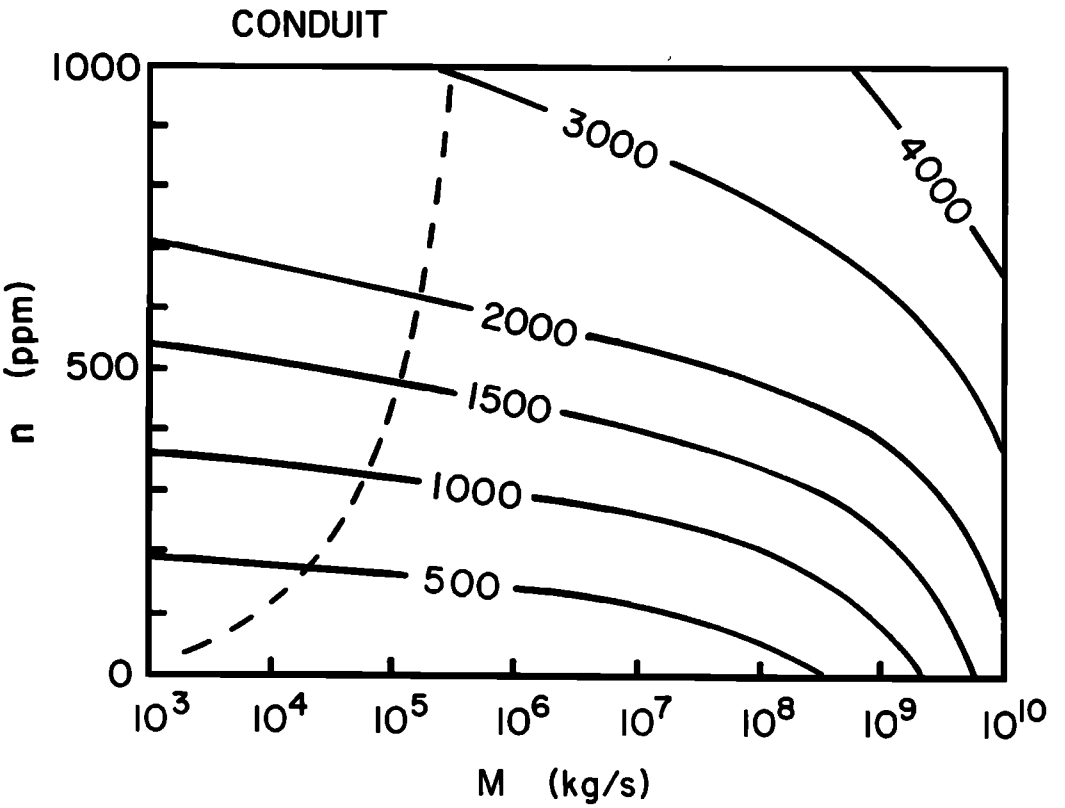

Fig. 17*a*

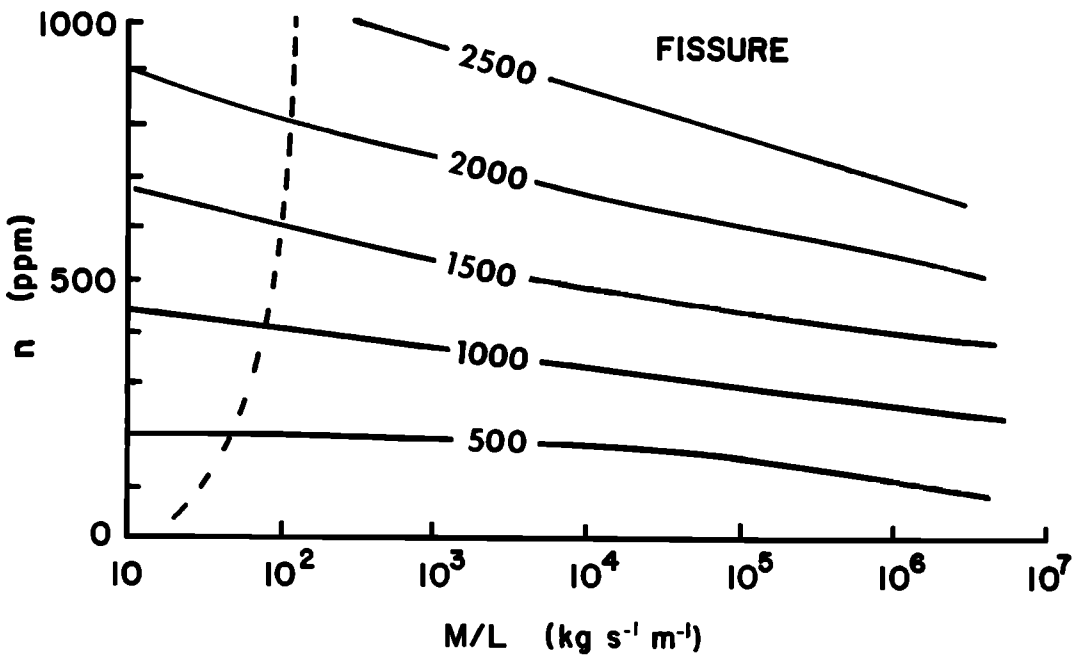

Fig. 17*b*

Fig. 17. Combinations of values of released CO content n and effusion rate required to produce a given maximum ejecta range for lunar eruptions in which the majority of the ejecta are submillimeter in size. Figure 17*a* is for circular conduits and Figure 17*b* for elongate fissures. In each case the solid curves are labeled by the maximum range in meters, and the dashed line marks the boundary between eruptions in which the eruption clouds are optically thick and those in which the clouds are optically thin. For eruptions to the left of the dashed line, pyroclasts land cool to form cinder cones; to the right of the line, ejecta land hot and coalesce to form lava flows.

significant acceleration by gas and for most of the path if they are submillimeter in size, since the acceleration occurs within a small region above the vent) and so their flight average time τ is given by the formula $\tau = (D/g)^{1/2}$. The number of objects in flight at any time is then $N\tau$, and they occupy a spatial region of radius D and height $D/2$ which is the envelope of all the parabolic trajectories and which has a volume close to D^3. Thus the number per unit volume in the cloud is $N\tau/D^3$ and

the typical separation is the cube root of the reciprocal of this quantity. Substituting for N and τ we have

$$S = d\left(\frac{\pi g^{1/2}\rho_l D^{2.5}}{6\sqrt{2}M}\right)^{1/3} \quad (65)$$

and hence for a circular vent,

$$\Lambda_c = \frac{5dg^{1/2}\rho_l D^{2.5}}{6\sqrt{2}M} \quad (66)$$

In the case of an elongate fissure the equivalent analysis yields Λ_f, where

$$6.9\Lambda_f = \frac{5\pi dg^{1/2}\rho_l D^{1.5}}{12\sqrt{2}(M/L)} \quad (67)$$

The above derivations have been based on the assumption that droplets in a cloud are distributed uniformly; this is not the case in general, and it will be valuable to deduce the relative thickness of the accumulating deposit and hence the relative density of the cloud just above it, as a function of distance from the vent. In the case of a circular vent from which ejecta are dispersed uniformly in all directions the relative amount of material ejected between elevations θ and $\theta + d\theta$ is proportional to $\cos\theta\, d\theta$. It lands in an annular region between ranges D and $D + dD$, which has area proportional to $D\,|dD|$, i.e., to $\sin 2\theta\,|\cos 2\theta|\, d\theta$, and so the relative thickness is proportional to $\cos\theta/\sin 2\theta\,|\cos 2\theta|$. This function has singularities at $\theta = 0°$ and 45°. The first of these is not too important, since it is probably unrealistic to imagine any ejecta being projected exactly horizontally from the vent: the most trivial surface irregularities at the edge of the vent will intercept such ejecta at once leading to progressive build-up of spatter structures. The singularity at 45° corresponds to the mathematical imposition of an exactly defined maximum range. Debris accumulating just at the maximum range will not build up a vertical outer wall to the deposit; instead, material will slump outward until a stable slope is reached. It is adequate to plot the above function for the relative thickness as a function of range at 2.5° steps of elevation as in Figure 18; the total deposit thickness at any range is made up of two components, the material arriving at elevation angles greater than and less than 45°. Clearly, ejecta accumulate preferentially near the vent and near the maximum range; roughly one eighth of the deposit volume lies within one tenth of the total deposit radius

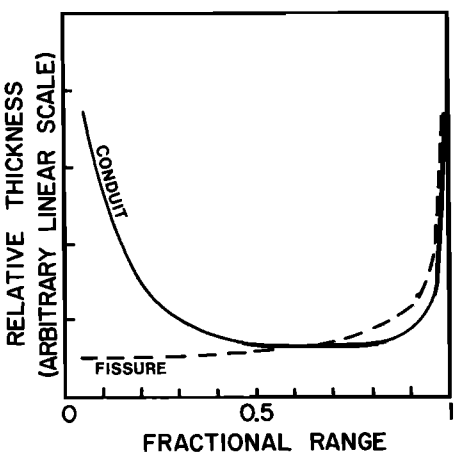

Fig. 18. The relative thicknesses of pyroclastic deposits from circular (solid curve) or elongate (dashed curve) lunar vents as a function of fractional distance to the maximum range of pyroclasts. See text for discussion.

TABLE 10. Values of the Velocity u_{st}, Gas Density ρ_g, and Largest Droplet Diameter d_{max} in a Stream of Gas and Small Droplets Ejected in a Lunar Strombolian Explosion as a Function of the Ratio of Ambient Pressure P to Initial Pressure P_0

P/P_0	u_{st}, m/s	ρ_g, kg/m^3	d_{max}, mm	X
0.8	169	1.3×10^{-2}	57	1.08
0.3	373	5.9×10^{-2}	127	1.5
0.1	486	2.6×10^{-3}	95	2.2
10^{-2}	612	4.3×10^{-4}	27	4.7
10^{-3}	676	7.4×10^{-5}	10	10
10^{-4}	710	1.3×10^{-5}	8	21
10^{-5}	730	2.1×10^{-6}	7	46

Also given is the approximate factor X by which the radius of the expanding gas cloud will have increased from its initial radius equal to that of the bursting bubble. See text for further details.

of the vent and one half of the deposit lies in the outer one tenth of the deposit radius. This is most important, since if the outer shell of the cloud is optically thick, little thermal radiation can escape from anywhere within it. We conclude that if Λ_c given by (66) is less than one tenth of the maximum radius of a circular deposit then the cloud from which that deposit forms is optically thick and the deposit accumulates with negligible cooling.

The same analysis can be applied to a fissure source. The simpler, elongate geometry leads to the result that the deposit thickness is proportional to $(\cos 2\theta)^{-1}$. Figure 18 shows the relative thickness as a function of fractional range; in this case the ejecta are mainly concentrated into the outer part of the deposit. The optical thickness criterion derived above is probably appropriate to this geometry also.

We can now apply these results to steady eruptions in which gas is released. First, consider the case where all the magmatic droplets are submillimeter in size, and assume that the mean droplet size is 10^{-1} mm. Figures 17*a* and 17*b* give maximum ejected droplet ranges as a function of gas content and effusion rate. For circular vents we use (66) to evaluate Λ_c at every point along the constant range curves in Figure 17*a* and so find the points at which Λ_c is one tenth the range. The locus of these points is shown as the dashed curve. To the left of this curve the ejecta cloud densities are such that the clouds are optically thin. Since thermal waves can pass through millimeter-sized silicate droplets in times of less than a second [*Sparks and Wilson*, 1976] and the flight time for droplets to reach as little as 500 m range on the moon is 25 s, the droplets can and do cool very efficiently and accumulate to form a pyroclastic deposit. To the right of the line the optical density of the ejecta cloud prevents cooling except in the outermost part of the cloud, and the accumulating ejecta are expected to coalesce into a lava flow. The implications are that if lunar magmas produce less than 1000 ppm of CO or similar gas, then (1) central vents cannot produce pyroclastic constructs at all unless mass eruption rates are less than 3×10^5 kg/s, (2) the diameters of such deposits (which are expected to be symmetrical) are not expected to be greater than 4 to 5 km, and (3) the diameters of the deposits are almost entirely determined by magma gas content and not mass eruption rate. The generalities of these conclusions would not change if the mean droplet size d were other than 10^{-1} mm (as long as it were not greater than a few millimeters, of course). Equation (66) shows that Λ_c is proportional to d/M, and so if the mean size were chosen to be larger or smaller by some specific factor, the boundary curve shown in Figure 17*a* would be moved to the right or left, respectively, parallel to the M axis, by the same factor.

TABLE 11. Approximate Values of the Maximum Ejection Velocity u_{st}, Range, and Particle Size d_{max}, for the Widely Dispersed Parts of Lunar Strombolian Deposits Given as a Function of n', the Fraction of the Ejected Material Which Consists of Gas

n'	u_{st}, m/s	Maximum Range, km	d_{max}, mm	$P:L$
0.1	478	141	7	1:200
0.2	676	282	10	1:500
0.4	956	564	14	1:1,300
0.9	1,434	1,269	21	1:18,000

The corresponding ratios of pyroclastic droplet mass to erupted lava mass $P:L$ are given for an average released magma CO content of 500 ppm by weight.

The equivalent procedure for fissure sources involves (67) and Figure 17*b*. The boundary curves for $d = 10^{-1}$ mm is shown as before, and the general conclusions are the same. The most surprising aspect of the calculation is that appreciable pyroclastic ramparts can only be built up along fissure sources if the effusion rate is very low, less than 50 to 150 kg s^{-1} m^{-1}. Equation (27), which gives the maximum depth of origin for a given effusion rate limited by cooling, implies that such eruptions cannot take place at all if the magma source is at a depth greater than about 2.5 km below the lunar surface for a magma viscosity of 10 Pa s and a density contrast of 200 kg/m^3. Even if the viscosity were as low as 1 Pa s and the density contrast as high as 400 kg/m^3, the maximum depth would be about 5 km, while an amount of magma superheating equal to the temperature difference between the solidus and liquidus temperatures (on which (27) was based) would be needed to allow the depth of origin to be as great as 10 km.

Finally, we treat the case where the ejected fragments are not predominantly submillimeter in size by reference to Figures 15*a* and 15*b*. The analysis proceeds in exactly the same way as in the preceding paragraphs. If the mean ejected clot size is less than about 10 mm, no combinations of gas content and effusion rate shown in the figures lead to deposits sufficiently cool to form pyroclastic structures. If the mean size is 0.1 m, the regions shown stippled are occupied by pyroclastic constructs (which can be up to 400 m in radius for central vents and up to 120 m in total width for fissures). If the mean size is 1 m (which is probably unrealistically large), the region of cinder formation extends into all of the zone to the left of the dotted line. Cones up to 6 or 8 km in diameter could be formed around central vents, and ridges up to 1 km in total width could be produced around fissure vents; very high effusion rates would be required, however.

E. Lunar Strombolian Eruptions

1. The strombolian explosion process. Figure 13 shows the variation of maximum bubble size with effusion rate and released CO content for lunar basalts; the circumstances under which catastrophic bubble growth occurs to fill the width of the conduit or fissure are shown. Once this condition is reached on the moon, the bubble will attempt to continue to occupy the full width of the vent, even if the vent lies in a topographic depression and opens out into a lava lake, since the gas in the bubble is striving to expend to infinite volume at the essentially zero pressure level of the lava lake surface. In practice, dynamic effects will limit the growth, since the finite viscosity of the magma will prevent it flowing out of the way arbitrarily quickly. The result will be an excess pressure in the bubble; indeed, when the typical dimension of the bubble is comparable to its depth below the surface, its detailed internal pressure distribution will be controlled completely by dynamic processes. This fact is partially taken into account by *Sparks'* [1978] computer program, since it includes inertial and viscous dynamic terms in the bubble growth equation; however, these terms effectively assume that the bubble is spherical (although the program correctly takes account of bubble deformation in finding the bubble rise velocity). A complete treatment would require very detailed analysis of the deformation of bubbles both by drag at the vent walls and by intertial forces, and we do not attempt this here. Instead, we assume that the excess pressures (above hydrostatic pressure) calculated by Sparks' program are an adequate indicator of the effective average pressures in a bubble nearing the surface of a lava lake. Values generally in the range 0.01 to 0.1 bar have been calculated by *Blackburn* [1977].

As a bubble approaches the surface, the liquid above it thins and attempts to flow out to the sides of the lava lake. In general, both the finite viscosity and the yield strength of the lava act to inhibit this flow (although the yield strength is probably negligible in lunar basalts). As is the case with terrestrial strombolian activity, some kind of instability must set in before the overlying liquid thickness goes to zero, and the liquid layer disrupts into pyroclasts. Examination of movie film of terrestrial strombolian activity suggests [*Blackburn*, 1977] that the largest pyroclasts have maximum dimensions of the order of several times the thickness of the liquid layer at the moment of disruption and minimum dimensions equal to the thickness. The same is almost certainly true on the moon, but we have no simple way of calculating what that thickness may be. There is the added complication that, as was the case with steady lunar fire fountains, the larger clots of liquid produced by disruption of the overlying layer may themselves contain small bubbles which attempt to expand, thus causing further disruption. Again, a wide range of final pyroclast sizes is expected with diameters as small as a few tens of microns.

2. Pyroclast velocities. As soon as the liquid layer above a rising bubble disrupts, the released gas begins to accelerate around the pyroclasts as an expansion wave propagates into the gas. Consideration of the liquid flow field around the bubble shows that all the pyroclasts have an initial upward velocity less than or comparable to the rise velocity of the bubble just before it bursts. The largest clasts may be only slightly accelerated subsequently by the drag forces resulting from the relative motion, while the smallest may be accelerated very quickly and remain locked to the gas motion for some time. The main difference between this process and its equivalent in the case of a steady lunar fire fountain is that in the latter case all of the liquid has essentially the same speed as the gas up to the moment of disruption and so all of the pyroclasts, especially the largest, have a much higher initial velocity at the start of the subsequent phase of particle sorting in the expanding gas cloud. Thus lunar strombolian explosions should lead to a higher degree of sorting for a given total range of particle sizes than lunar fire fountain eruptions.

If the velocities of the coarsest ejecta are approximated by the rise speeds of bubbles near the surface, then Sparks' program shows that they will be in the range 1 to 3 m/s for bubbles with diameters from 1 to 10 m. Such ejecta would only be thrown to distances of a few meters. If, on the other hand, the

smallest droplets stay locked to the gas long enough for the gas pressure to decrease by a few orders of magnitude, then these droplets can reach high speeds and large ranges [*Housley*, 1978]. Let u_{st} be the final velocity of the spray of gas and small droplets as a result of the gas expansion from an initial temperature T_0 and pressure P_0 to a final pressure P, and let n' be the weight fraction of gas in the expanding mixture. It is probably safe to assume that the gas expansion is adiabatic, since most of the decompression must occur quickly over a distance equal to a few times the diameter of the bursting bubble. The small spatial scale and lack of a surrounding medium mean that the potential energy and friction terms can be neglected in (1); use of (10) then leads to

$$u_{st}^2 = \frac{2n_\gamma' Q T_0}{(\gamma - 1)m}\left[1 - \left(\frac{P}{P_0}\right)^{(\gamma-1)/\gamma}\right] \tag{68}$$

while (10) itself implies that the gas density ρ_g decreases from its initial value ρ_{g0} so that

$$\rho_g = \rho_{g0}(P/P_0)^{1/\gamma} \tag{69}$$

where ρ_{g0} is given by (5) as mP_0/QT_0. If we take as typical values $P_0 = 0.05$ bars, $T_0 = 1200$ K and insert the constants, we find $\rho_{g0} = 1.5 \times 10^{-2}$ kg/m^3. The value to be adopted for n' is a function of the bubble bursting geometry, since the weight fraction of the ejecta which consists of gas is equal to the ratio of the mass of gas in the bubble to the sum of the masses of the gas and that part of the liquid surface layer which is converted to pyroclastic droplets. Again, it is hard to specify a typical value. For terrestrial strombolian explosions, n' ranges from 0.1 to 0.3 in many cases [*Blackburn et al.*, 1976] but can be in excess of 0.9 [*Chouet et al.*, 1974]. We initially select a value of 0.2; Table 10 then show some values of u_{st} and ρ_g as a function of decreasing (P/P_0). Also shown are the diameters d_{max} of the dense (3000 kg/m^3) droplets which have terminal velocities in the gas just equal to the gas velocity, calculated by the method of *Walker et al.* [1971]. Only droplets a few times smaller than this size can remain locked to the gas, though it is clear that if the lunar magma is thoroughly fragmented this could include the majority of pyroclasts.

Alternative values of n' change the velocities and sizes of supported droplets, u_{st} varying as $\sqrt{n'}$ and d_{max} varying in approximately the same way. If values several times smaller than 0.2 are assumed, the ultimate velocity is still of order a few hundred meters per second, and the supported droplets can be up to at least several millimeters in size. It is clearly hard to avoid these droplets being dispersed over regions with radii of order many tens of kilometers on the moon. If values of n' up to about 0.9 are allowed, the above particle sizes are doubled, and ranges are quadrupled. However, if n' is large, this simply implies that only a small part of the magma is blasted away in each explosion; the rest effuses to form a lava flow. Table 11 summarizes these results by giving maximum values of particle size, ejection velocity, and deposit radius for several values of n' calculated at $P/P_0 = 10^{-3}$. Also given are the ratios of pyroclast mass to lava mass implied if the average exsolved magma CO content is 500 ppm.

F. *Synthesis of Lunar Eruption Styles*

A number of the results of the previous sections on various types of lunar basaltic eruption are not mutually exclusive, especially in terms of the interaction of the restrictions imposed by (1) consideration of clast cooling rates and (2) the presence or absence of the strombolian explosion style. It is possible to summarize the results contained in Figures 13 to 18 in the following manner:

1. Conduit sources.

In a steady eruption (i.e., $M \gg 100$ kg/s) in which magma is disrupted into mainly submillimeter droplets the following occur:

1. For $M > 10^5$ kg/s all ejecta coalesce into a lava flow fed from a circular lava pool with radius commonly up to 3 km; pool radius increases with both M and n (Figure 17*a*).
2. For $\sim 100 < M < 10^5$ kg/s, ejecta form a cooled circular blanket up to 2.5-km radius; radius increases mainly with n (Figure 17*a*); deposit thickness greatest near vent and at maximum range (Figure 18); lava flow formation from vent is possible but unlikely.

In a steady eruption (i.e., $M \gg 100$ kg/s) in which magma is disrupted into clots in the size range 10 mm to 1 m the following occur:

1. For $M > 10^7$ kg/s for all n or $n > \sim 200$ ppm for all M, all ejecta coalesce into a flow fed from a circular pool with radius commonly up to 2 or 3 km; pool radius depends mainly on M (Figure 15*a*).
2. For $M > 10^7$ kg/s and $n < \sim 200$ ppm, ejecta form a cooled circular blanket with radius up to 300 m; blanket radius increases with M and decreases with n (Figure 15*a*); deposit thickness greatest near vent; lava flow formation is possible but unlikely.

In the case of strombolian activity (i.e., $M \lesssim 100$ kg/s), lava flow from vent is quite likely; coarse clots accumulate within 10 to 20 m of vent to form spatter cone; submillimeter fines expelled to many tens of kilometers; clasts in the size range 1 to 10 mm may collect into cinder cone within a few hundred meters of vent.

2. Fissure sources.

In a steady eruption (i.e., $M/L \gg 100$ *kg s*$^{-1}$ *m*$^{-1}$) in which magma is disrupted into mainly submillimeter droplets, all ejecta coalesce into a flow fed from a zone parallel to the fissure and up to 4 km in total width; zone width increases mainly with n (Figure 17*b*).

In a steady eruption (i.e., $M/L \gg 100$ kg s^{-1} m^{-1}) in which magma is disrupted into clots mainly in the size range 10 mm to 1 m the following occur:

1. For $M/L > 3 \times 10^4$ kg s^{-1} m^{-1} for all n or $n > \sim 100$ ppm for all M/L, all ejecta coalesce into a flow fed from a zone parallel to the fissure and up to 2 km wide; zone width increases mainly with M/L (Figure 15*b*).
2. For $M/L < 3 \times 10^4$ kg s^{-1} m^{-1} and $n < \sim 100$ ppm, ejecta form cool blanket parallel to the fissure and up to 150 m wide; blanket width increases with M/L and decreases with n (Figure 15*b*); blanket thickness is greatest near maximum range (Figure 18); lava flow formation is possible but unlikely.

In the case of strombolian activity (i.e., $M/L \lesssim 100$ kg s^{-1} m^{-1}), lava flow from vent is quite likely; coarse clots accumulate within 10 to 20 m to form spatter ridge on either side of the fissure; submillimeter fines ejected to many tens of kilometers; clasts in the size range 1 to 10 mm may collect into cinder ridge within a few hundred meters of fissure.

VI. CONCLUSIONS

A. *General*

1. Relatively simple mathematical models of the motion of gas/liquid mixtures, such as those proposed by *McGetchin and Ullrich* [1973] and *Pai et al.* [1978] and applied to terres-

trial acid eruptions by *Wilson et al.* [1980] are adequate to treat basaltic eruptions provided that allowance is made for the coalescence of gas bubbles and that realistic geological and petrochemical constraints are applied to the numerical values of the variables involved.

2. Gas exsolution from magmas on the earth and moon (and Mars) only occurs at relatively shallow depths (commonly less than 2 km for terrestrial and lunar basalts). As a result it is generally convenient to consider separately the rise of bubble-free magmatic liquid at depth in a planetary crust and the more complex motions which occur near the surface as gas is exsolved.

3. A lower limit is set to the width of the dike or conduit up which a magma can rise from a given depth, either by the presence of a finite yield strength in the magma or by the need to avoid excessive cooling of the magma during its ascent. The latter constraint is controlled mainly by the magma viscosity. For a wide range of magma types it is found that if the yield strength at depth is greater than a few hundred N/m^2, then yield strength rather than viscosity will limit the ability of the magma to erupt.

4. Bubble coalescence, leading to intermittent explosive activity of strombolian style, will occur in any magma near the surface if the rise speed is sufficiently slow or the viscosity (and yield strength) are sufficiently small. For the commonly occurring basalts on both the earth and moon the rise speed in the crust must be greater than 0.5 to 1 m/s if strombolian activity is to be avoided and relatively steady fire fountaining is to take place.

B. Earth

1. For terrestrial basalts commonly having viscosities not less than 10^2 Pa s and negligible yield strengths, dike or conduit widths in the range 0.2 to 0.6 m are needed to allow eruptions from depths between 500 m and 20 km. Corresponding minimum mass eruption rates lie in the range 10 to 300 kg/s for isolated central conduits and in the range 30 to 500 kg s^{-1} m^{-1} length of fissure for elongate vents. To accommodate the output rates of 3×10^4 kg s^{-1} m^{-1} estimated for the Columbia River flood basalt eruptions [*Swanson et al.*, 1975], fissures up to about 4 m wide would be needed.

2. Fire fountain height is dictated by the vertical velocity of the magma/gas dispersion emerging through the vent, and both quantities increase with increasing magma gas content, increase with increasing mass eruption rate, and decrease with increasing magma viscosity: see Figures 7*a* and 7*b*, Tables 7 and 8, and equation (33). Fire fountains up to 500 m high imply the release of up to about 0.4 wt % of water from the magma, corresponding to initial water contents up to about 0.6 wt %.

C. Moon

1. Lunar basaltic eruptions differed from their current terrestrial counterparts in that the magmatic liquids were produced at relatively great depths and were relatively dense compared to the upper lunar crust; however, consideration of the topography of mare basins, based on the treatment of *Solomon* [1975], shows that the effective density contrast driving lunar eruptions was similar to the actual density contrast driving terrestrial basaltic eruptions.

2. The main volatile released from lunar magmas was probably carbon monoxide, produced in amounts up to several hundred ppm [*Housley*, 1978]—proportionately less by more than an order of magnitude than is common in terrestrial magmas. However, the much greater energy release per unit mass from this gas as it decompressed to the near-zero ambient lunar atmospheric pressure, coupled with the fact that both vertical and horizontal expansion of the gas must have occurred, imply a much more efficient use of the available gas on the moon than on the earth. The gas volume fraction would reach 0.75, leading to magma disruption, at depths of 14 and 41 m for CO contents of 250 and 750 ppm, respectively; some measure of magma disruption must always have taken place in lunar eruptions unless either the gas content were truly zero or the magma possessed an appreciable yield strength.

3. The differences between terrestrial and lunar magma rheologies and crustal environments do not lead to gross differences between the effusion rates expected on these two planets through fissures or conduits of a given size (Tables 3–6). Consequently, the recognition of high effusion rate features such as long lava flows and sinuous rilles on the moon implies only that the tectonic and other forces associated with the onset of some lunar eruptions were such as to allow wide fissures or conduits to form. Since a single, high effusion rate, large volume eruption can bury the products of many earlier, smaller events it is difficult to assess the relative frequency of high- and low-effusion rate eruptions on the Moon from photographs alone. It is possible, however, that the common occurrence of high effusion rate eruptions could explain the apparent absence of large lunar basaltic shield volcanoes [*Head and Gifford*, 1980]; recognizable individual shields can only be built up when the mean distance flowed by lavas from one source area is substantially less than the mean spacing between sources.

4. The surface widths of elongate fissure vents need be no wider than 10 m to permit the occurrence of mass eruption rates up to 10 times larger than those proposed for terrestrial flood basalt eruptions; effusion rates 100 times larger could be accommodated by 25-m-wide vents. As a result, elongate fissurelike structures with widths of many tens to hundreds of meters commonly identified as lunar vents [*Schultz*, 1976; *Head*, 1976] are rarely likely to represent the true vent sizes directly. These structures may be the results of collapse around a vent after eruption ceases or may be produced by accumulation of pyroclastic debris in some circumstances.

5. In order to determine the total volume of partial melt separated from the source area one must know both the volume emplaced on the lunar surface [*Head*, 1975] and the volume emplaced between the source and the surface [*Head*, 1980] in the form of dikes, sills, and other intrusive bodies. Dikes of dense basaltic magma could readily have penetrated the relatively low-density lunar crust to some extent even in the absence of impact-excavated basins provided the primary source regions were at sufficient depth. The greater the depth of the source region, the closer to the surface can a liquid of given density rise. As the lunar lithosphere thickened with time and the lunar mantle cooled during the period of mare basin filling, source regions for partial melts probably migrated to greater depths, and eruptions of dense mare basalts into topographic depressions became more likely in terms of the hydrostatics of the events. If it is accepted as likely that the available volumes of partial melt decreased with time during lunar history, then it follows that dikes should form a larger percentage of the deep crust than the near-surface crust and that the total volume of dike material at depth should be

substantially greater than the inferred volume of basaltic lava actually erupted onto the lunar surface [*Head,* 1975].

6. In cases where dense, rising liquids failed to reach the surface but encountered relatively incompetent layers, sills or shallow magma reservoirs could have been formed in the same way as on earth. It is conceivable that later eruptions could have taken place from any such reservoirs large enough to avoid rapid cooling if either later tensional tectonic adjustments provided easy pathways to the surface or chemical reactions produced a build-up of gas pressure which led to fracturing of the overburden. In the latter case, the solubilities of all the likely gas species are such that the reservoirs would have to have been within about 2 km of the surface.

7. Considerations of the details of basaltic eruption processes on the moon lead to the prediction of several types of volcanic landforms. We discuss elsewhere the correlation of these landforms with specific lunar features (J. W. Head and L. Wilson, manuscripts in preparation, 1980).

Circular pyroclastic blankets formed around a central vent: These should be low and wide relative to terrestrial counterparts (but the ratio height/width is proportional to eruption duration for fixed M and n). Blankets which are relatively thick both near the vent and near the maximum range (domelike or shieldlike) and which have a well-defined outer edge would be the products of eruptions in which most of the magma was disrupted into submillimeter droplets and in which M lay in the range 10^2 to 10^5 kg/s; blanket radii up to 2.4 km would be expected for released gas contents, n, up to 750 ppm. Blankets which are relatively thick only near the vent (low cone shape) and have radii up to 300 m would be products of eruptions in which all the magma was disrupted into clots larger than several millimeters, in which n was less than about 200 ppm and in which M lay in the range 10^2 to 10^7 kg/s; such low, conelike features could be wider (up to 1.5 to 2 km radius for M up to 10^6 kg/s) if magma fragments were concentrated into the size range 1 to 10 mm. In all the above cases, lava flows could easily be absent; flows would be formed, however, if either M or n became small at any stage during the eruption.

Circular 'regions' up to 3 km radius around a central vent which are the sources of major lava flows: These would be formed for M greater than 10^5 kg/s if most of the magma were disrupted into submillimeter droplets or for M greater than 10^7 kg/s if the magma disrupted mainly into clots larger than a few millimeters. We shall explore elsewhere the possibility that these regions are the circular depressions that appear to be the sources of some sinuous rilles.

Circular pyroclastic cones, commonly less than 50 m in radius, acting as the sources of minor lava flows: These would mark sites of low-effusion rate conduit eruptions. Values of M would have been nominally less than about 100 kg/s, but taking account of the uncertainties in the calculations may have been up to a few hundred kilograms per second. Such features should commonly be surrounded by very thin pyroclastic blankets of submillimeter droplets extending out to many tens of kilometers.

Elongate cinder or spatter ridges: These should be very rare unless they are narrower than about 1 km. Ridges up to 150 m wide and highest near their outer edges could be formed by steady fissure eruptions in which magma was disrupted mainly into clots larger than a few millimeters provided M/L was less than 3×10^4 kg s^{-1} m^{-1} and n was less than about 100 ppm. Wider ridges up to 1 km wide could be formed for the same ranges of values of M/L and n if magma were disrupted mainly into clasts in the 1 to 10 mm size range. In both the above cases, lava flows would commonly be absent. However, ridges up to about 500 m wide with associated lava flows could be formed by strombolian activity with M/L less than a few hundred kg s^{-1} m^{-1} provided the explosions disrupted the magma into clots mainly in the 1 to 10 mm size range. Otherwise, strombolian activity from fissure sources would build very narrow spatter ridges (up to about 40 m wide) from coarse ejecta and distribute a thin blanket of submillimeter droplets for distances up to tens of kilometers.

Elongate regions up to 4 km wide which are the sources of major lava flows: These would be associated with the great majority of high effusion rate eruptions from fissures. The direction of drainage of lava flows away from these source regions would depend on local topography. Where such drainage was along the direction of the controlling fissure, a pyroclastic rampart could be built up parallel to the fissure at the maximum range of the ejected material due to deposition of relatively cool clasts in the optically thin outermost part of the ejecta cloud. Where lava drainage was at right angles to the fissure direction, any cool clasts would be rafted away on the flow.

Dark mantle deposits: These should take the form of very extensive but thin deposits; diameters could commonly be up to 50 km and might be as large as 200 km. Sources would either be vents from which steady eruptions occurred at high effusion rates but only a small fraction (of the order of 1%) of the magma disrupted into submillimeter droplets (Figure 16) or low effusion rate eruptions in which strombolian activity occurred. Thus dark mantle deposits are not particularly diagnostic of high or low effusion rates, high or low magma gas contents, or geometric shape of source vent. It can, however, be asserted that the total mass of material ejected into a dark mantle deposit must consist of submillimeter droplets and must be much less than the mass of material ejected into near-vent flows or pyroclastic structures: by a factor of order 100 in the case of high effusion rate eruptions and by a factor of order 1000 in the case of strombolian explosions. Dark halo craters of the Alphonsus type appear to be produced by a different eruption process, one analogous to terrestrial vulcanian explosive activity [*Head and Wilson,* 1979].

Hybrid sources: We stress the fact that where a vent region is fissure-controlled but only parts of the fissure system are wide enough at depth to allow rapid magma rise, the result will be a series of relatively isolated vents aligned along the fissure. In these cases, and in any other cases where the typical ranges of ejecta are much greater than the active length of an elongate vent, it will be much more accurate to treat the system as one or more central conduit sources rather than a fissure source.

Acknowledgments. This research was supported by National Aeronautics and Space Administration grant NGR-40-002-116 from the Planetary Programs Office. Additional funds were provided by the William F. Marlar Memorial Foundation and by the Department of Geological Sciences, Brown University. We gratefully acknowledge the constructive comments of three anonymous reviewers. The help of Ruth Gorski (drafting), Ed Robinson (programming), and Nancy Christy and Sally Bosworth (manuscript preparation) is gratefully acknowledged. R. S. J. Sparks kindly provided us with a copy of his bubble rise computer program. This paper constitutes Contribution 43 of the Basaltic Volcanism Study Project. The project is organized and administered by the Lunar and Planetary Institute/Universities Space Research Association under contract NSR 09-051-001 with the

National Aeronautics and Space Administration. This paper is dedicated to Thomas R. McGetchin whose enthusiasm for volcanoes, and understanding of how they work, led to both authors' interest in the subject. His early work (McGetchin and Ullrich, 1973) formed an important foundation for our calculations.

REFERENCES

Aki, K., M. Fehler, and S. Das, Source mechanisms of volcanic tremor: Fluid-driven crack models and their application to the 1963 Kilauea eruption, *J. Volcanol. Geotherm. Res., 2,* 259–287, 1977.

Blackburn, E. A., Some aspects of explosive volcanism on the earth, moon and Mars, Ph.D. thesis, Univ. of Lancaster, U. K., 1977.

Blackburn, E. A., L. Wilson, and R. S. J. Sparks, Mechanisms and dynamics of strombolian activity, *J. Geol. Soc. London, 132,* 429–440, 1976.

Bottinga, Y., and D. F. Weill, The viscosity of magmatic silicate liquids: A model for calculation, *Am. J. Sci., 272,* 438–475, 1972.

Burnham, C. W., and N. F. Davis, The role of H_2O in silicate melts, II, Thermodynamic and phase relations in the system $NaAlSi_3O_8$-H_2O to 10 kilobars, 700° to 1100°C, *Am. J. Sci., 274,* 902–940, 1974.

Chouet, B., N. Hamisevicz, and T. R. McGetchin, Photoballistics of volcanic jet activity at Stromboli, Italy, *J. Geophys. Res., 79,* 4961–4976, 1974.

Cole, B. N., H. M. Bowers, and F. Hobbs, A theory for the high-speed flow of gas-solids mixtures under conditions of equilibrium and constant frictional lag, Fluid Mechanics and Measurements in Two Phase Flow Systems, *Proc. Inst. Mech. Eng., 184*(3c), 59–66, 1969.

Cooper, M. R., R. L. Kovach, and J. S. Watkins, Lunar near-surface structure, *Rev. Geophys. Space Phys., 12,* 291–308, 1974.

Davies, P. A., and A. Stephenson, The ages of the lunar maria and the filling of the mare basins, *Phys. Earth Planet. Inter., 14,* P13–P16, 1977.

Delaney, P. T., and D. D. Pollard, Solidification of magma during flow in a dike, *Am. J. Sci.,* in press, 1980.

Elder, J., *The Bowels of the Earth,* 222 pp., Oxford University Press, New York, 1976.

Fedotov, S. A., Geophysical data on deep-seated magmatic activity below Kamchatka and an estimate of the forces that cause the rise of magmas into volcanoes, *Int. Geol. Rev., 6,* 661–670, 1977*a*.

Fedotov, S. A., Mechanism of deep-seated magmatic activity below island-arcs volcanoes and similar structures, *Int. Geol. Rev., 6,* 671–680, 1977*b*.

Fedotov, S. A., Ascent of basic magmas in the crust and the mechanism of basaltic fissure eruptions, *Int. Geol. Rev., 20,* 33–48, 1978.

Hardee, H. C., and D. W. Larson, Viscous dissipation effects in magma conduits, *J. Volcanol. Geotherm. Res. 2,* 299–308, 1977.

Head, J. W., Lunar mare deposits: Areas, volumes, sequence, and implication for melting in source areas, in *Origins of Mare Basalts and Their Implications for Lunar Evolution,* pp. 66–69, The Lunar Science Institute, Houston, Tex., 1975.

Head, J. W., Lunar volcanism in space and time, *Rev. Geophys. Space Phys., 14,* 265–300, 1976.

Head, J. W., Lava flooding of early planetary crusts: Geometry, thickness, and volumes of flooded lunar impact basins, submitted to *Moon Planets,* 1980.

Head, J. W., and A. Gifford, Lunar mare domes: Classification and modes of origin, *Moon Planets, 22,* 235–258, 1980.

Head, J. W. and L. Wilson, Alphonsus-type dark-halo craters: Morphology, morphometry and eruption conditions, *Proc. Lunar Planet. Sci. Conf., 10th,* 2861–2897, 1979.

Heiken, G., and D. S. McKay, A model for the eruption behavior of a volcanic vent in Eastern Mare Serenitatis, *Proc. Lunar. Sci. Conf., 8th,* 3243–3255, 1977.

Holloway, J. R., Fluids in the evolution of granitic magmas: Consequences of finite CO_2 solubility, *Geol. Soc. Am. Bull., 87,* 1513–1518, 1976.

Housley, R. M., Modelling lunar eruptions, *Proc. Lunar Planet. Sci. Conf., 9th,* 1473–1484, 1978.

Hsieh, D. Y., and M. S. Plesset, On the propagation of sound in a liquid containing gas bubbles, *Phys. Fluids, 4,* 970–975, 1961.

Hulme, G., and G. Fielder, Effusion rates and rheology of lunar lavas, *Philos. Trans. R. Soc. London, Ser. A., 285,* 227–234, 1977.

Jaeger, J. C., Thermal effects of intrusions, *Rev. Geophys. Space Phys., 2*(3), 1964.

Johnson, A. M., and D. D. Pollard, Mechanics of growth of some laccolithic intrusions in the Neary Mountains, Utah, I, Field observations, Gilbert's model, physical properties and flow of the magma, *Tectonophysics, 18,* 261–309, 1973.

Kesson, S. E., and D. H. Lindsley, Mare basalt petrogenesis: A review of experimental studies, *Rev. Geophys. Space Phys., 14,* 361–373, 1976.

Kieffer, S. W., Sound speed in liquid-gas mixtures: Water-air and water-steam, *J. Geophys. Res., 82,* 2895–2904, 1977.

Kliegel, J. R., Gas particle nozzle flows, *Symp. Int. Combust. Proc.,* 811–826, 1963.

Kushiro, F., H. S. Yoder, and B. O. Mysen, Viscosities of basalt and andesite melts at high pressures, *J. Geophys. Res., 81,* 6351–6356, 1976.

Macdonald, G. A., *Volcanoes,* 510 pp., Prentice-Hall, Englewood Cliffs, N. J., 1972.

Marsh, B. D., On the cooling of ascending andesitic magma, *Philos. Trans. R. Soc. London, Ser. A, 288,* 611–625, 1978.

Marsh, B. D., and L. H. Kantha, On the heat and mass transfer from an ascending magma, *Earth. Planet. Sci. Lett., 39,* 435–443, 1978.

McGetchin, T. R., and W. G. Ullrich, Zenoliths in maars and diatremes with inferences for the moon, Mars and Venus, *J. Geophys. Res., 78,* 1833–1853, 1973.

Moore, J. G., and J.-G. Schilling, Vesicles, water and sulphur in Reykjanes Ridge basalts, *Contrib. Mineral. Petrol., 41,* 105–118, 1973.

Murase, T., and A. R. McBirney, Viscosity of lunar lavas, *Science, 167,* 1491–1493, 1970.

Murase, T., and A. R. McBirney, Properties of some common igneous rocks and their melts at high temperature, *Geol. Soc. Am. Bull., 84,* 3563–3592, 1973.

Mutch, T. A., R. E. Arvidson, K. L. Jones, J. W. Head, and R. S. Saunders, *The Geology of Mars,* 436 pp., Princeton University Press, Princeton, N.J., 1976.

Mysen, B. O., The solubility of H_2O and CO_2 under predicted magma genesis conditions and some petrological and geophysical implications, *Rev. Geophys. Space Phys., 15,* 351–361, 1977.

Pai, S. I., Y. Shu, and J. A. O'Keefe, Similar explosive eruptions of lunar and terrestrial volcanoes, *Proc. Lunar Planet. Sci. Conf., 9th,* 1485–1508, 1978.

Papike, J. J., F. N. Hodges, A. E. Bence, M. Cameron, and J. M. Rhodes, Mare basalts: Crystal chemistry, mineralogy, and petrology, *Rev. Geophys. Space Phys., 14,* 475–540, 1976.

Pinkerton, H., and R. S. J. Sparks, Field measurements of the rheology of lava, *Nature, 276,* 383–385, 1978.

Pollard, D. D., On the form and stability of open hydraulic fractures in the earth's crust, *Geophys. Res. Lett., 3,* 513–516, 1976.

Pollard, D. D., and O. H. Muller, The effects of gradients in regional stress an magma pressure on the form of sheet intrusions in cross section, *J. Geophys. Res., 81,* 975–984, 1976.

Popov, V. S., Mechanics of intrusion of thin dykes and sills, *Izv. Akad. Nauk SSR Ser. Geol., 10,* 1973.

Ramberg, H., Gravity, in *Deformation and the Earth's Crust as Studied by Centrifuged Models,* 214 pp., Academic, New York, 1967.

Richter, D. H., J. P. Eaton, K. J. Murata, W. A. Ault, and H. L. Krivoy, Chronological narrative of the 1959–60 eruption of Kilauea Volcano, Hawaii, *Geol Surv. Prof. Pap. U.S., 537-E,* 1970.

Ringwood, A. E., and S. E. Kesson, A dynamic model for mare basalt petrogenesis, *Proc. Lunar Sci. Conf., 7th,* 1697–1722, 1976.

Rudinger, G., Some properties of shock relaxation in gas flows carrying small particles, *Phys. Fluids, 7,* 658–663, 1964.

Saffman, P. G., On the stability of flow in a dusty gas, *J. Fluid Mech., 13,* 120–128, 1967.

Sato, M., Oxygen fugacity and other thermochemical parameters of Apollo 17 high Ti basalts and their implications on the reduction mechanism, *Proc. Lunar Sci. Conf., 7th,* 1323–1344, 1976.

Sato, M., The driving mechanism of lunar pyroclastic eruptions inferred from the oxygen fugacity behavior of Apollo 17 orange glass, *Eos Trans. AGU, 58,* 425, 1977.

Schlichting, H., *Boundary Layer Theory,* McGraw-Hill, New York, 1968.

Schultz, P. H., *Moon Morphology,* 612 pp., University of Texas Press, Austin, 1976.

Self, S., L. Wilson, and I. A. Nairn, Vulcanian eruption mechanisms, *Nature, 277,* 440–443, 1979.

Shaw, H. R., Rheology of basalt in the melting range, *J. Petrol., 10,* 510–535, 1969.

Shaw, H. R., Viscosity of magmatic silicate liquids: An empirical method of prediction, *Am. J. Sci., 272,* 870–893, 1972.

Shaw, H. R., and D. A. Swanson, Eruption and flow rates of flood basalts, in *Proceedings, 2nd Columbia River Basalts Symposium,* edited by E. H. Gilmour and D. Stradling, Eastern Washington State College Press, Cheney, 1970.

Shaw, H. R., T. L. Wright, D. L. Peck, and R. Okamura, The viscosity of basaltic magma: An analysis of field measurements in Makaopuhi lava lake, Hawaii, *Am. J. Sci., 266,* 225–264, 1968.

Solomon, S. C., Mare volcanism and lunar crustal structure, *Proc. Lunar Sci. Conf., 6th,* 1021–1042, 1975.

Soo, S. L., Gas dynamic processes involving suspended solids, *AIChE J., 7,* 384–391, 1961.

Soo, S. L., *Fluid Dynamics of Multiphase Systems,* 524 pp., Blaisdell, Waltham, Mass., 1967.

Sparks, R. S. J., The dynamics of bubble formation and growth in magmas: A review and analysis, *J. Volcanol. Geotherm. Res., 3,* 1–37, 1978.

Sparks, R. S. J., and H. Pinkerton, Effect of degassing on the rheology of basalt lava, *Nature, 276,* 385–386, 1978.

Sparks, R. S. J., and L. Wilson, A model for the formation of ignimbrites by gravitational column collapse, *J. Geol. Soc. London, 132,* 441–451, 1976.

Sparks, R. S. J., H. Pinkerton, and R. Macdonald, The transport of xenoliths in magmas, *Earth Planet. Sci. Lett., 35,* 234–238, 1977.

Sparks, R. S. J., L. Wilson, and G. Hulme, Theoretical modeling of the generation, movement, and emplacement of pyroclastic flows by column collapse, *J. Geophys. Res., 83,* 1727–1739, 1978.

Steinberg, G. S., and A. S. Steinberg, On possible causes of volcanic tremor, *J. Geophys. Res., 80,* 1600–1604, 1975.

Swanson, D. W., T. L. Wright, and R. T. Helz, Linear vent systems and estimated rates of magma production and eruption for the Yakima basalt on the Columbia Plateau, *Am. J. Sci., 275,* 877–905, 1975.

Thorarinsson, S., The Lakagigar eruption of 1783, *Bull. Volcanol., 33,* 910–929, 1969.

Thorarinsson, S., and G. E. Sigvaldason, The eruption in Askja, 1961: A preliminary report, *Am. J. Sci., 260,* 641–651, 1962.

Thorarinsson, S., S. Steinthorsson, Th. Einarsson, H. Kristmannsdottir, and N. Oskarsson, The eruption on Heimaey, Iceland, *Nature, 241,* 372–375, 1973.

Wadge, G., The storage and release of magma on Mount Etna, *J. Volcanol. Geotherm. Res., 2,* 361–384, 1977.

Wadge, G. The variation of magma discharge during basaltic eruptions, submitted to *J. Geophys. Res.,* 1980.

Walker, G. P. L., L. Wilson, and E. L. G. Bowell, Explosive volcanic eruptions: I, The rate of fall of pyroclasts, *Geophys. J. R. Astron. Soc., 22,* 377–383, 1971.

Weertman, J., Velocity at which liquid-filled cracks move in the earth's crust or in glaciers, *J. Geophys. Res., 76,* 8544–8553, 1971*a*.

Weertman, J., Theory of water-filled crevasses in glaciers applied to vertical magma transport beneath oceanic ridges, *J. Geophys. Res., 76,* 1171–1183, 1971*b*.

Wilson, L., Explosive volcanic eruptions, III, Plinian eruption columns, *Geophys. J. R. Astron. Soc., 45,* 543–556, 1976.

Wilson, L., Relationships between pressure, volatile content and ejecta velocity in three types of volcanic explosion, *J. Volcanol. Geotherm. Res., 8,* 297–313, 1980.

Wilson, L., R. S. J. Sparks, and G. P. L. Walker, Explosive volcanic eruptions, IV, The control of magma properties and conduit geometry on eruption column behavior, *Geophys. J. R. Astron. Soc., 63,* 117–148, 1980.

(Received February 21, 1980;
revised August 7, 1980;
accepted August 29, 1980.)